Journal of Geophysical Research: Solid Earth

RESEARCH ARTICLE
10.1002/2017JB014770

Special Section:
Stress at Active Plate Boundaries - Measurement and Analysis, and Implications for Seismic Hazard

Deformation of the Pacific/North America Plate Boundary at Queen Charlotte Fault: The Possible Role of Rheology

U. S. ten Brink[1], N. C. Miller[1], B. D. Andrews[1], D. S. Brothers[2], and P. J. Haeussler[3]

[1]U.S. Geological Survey, Woods Hole, MA, USA, [2]U.S. Geological Survey, Santa Cruz, CA, USA, [3]U.S. Geological Survey, Anchorage, AK, USA

Key Points:
- Pacific-North America plate boundary is located on the ocean-continent boundary, an unusual location for continental transforms
- The bimaterial contrast across the plate boundary focuses the deformation on a single narrow fault
- A scenario for the development of the plate boundary is proposed

Correspondence to:
U. S. ten Brink,
utenbrink@usgs.gov

Citation:
ten Brink, U. S., Miller, N. C., Andrews, B. D., Brothers, D. S., & Haeussler, P. J. (2018). Deformation of the Pacific/North America plate boundary at Queen Charlotte Fault: The possible role of rheology. *Journal of Geophysical Research: Solid Earth*, *123*, 4223–4242. https://doi.org/10.1002/2017JB014770

Received 24 JUL 2017
Accepted 24 MAR 2018
Accepted article online 30 MAR 2018
Published online 8 MAY 2018

Abstract The Pacific/North America (PA/NA) plate boundary between Vancouver Island and Alaska is similar to the PA/NA boundary in California in its kinematic history and the rate and azimuth of current relative motion, yet their deformation styles are distinct. The California plate boundary shows a broad zone of parallel strike slip and thrust faults and folds, whereas the 49-mm/yr PA/NA relative plate motion in Canada and Alaska is centered on a single, narrow, continuous ~900-km-long fault, the Queen Charlotte Fault (QCF). Using gravity analysis, we propose that this plate boundary is centered on the continent/ocean boundary (COB), an unusual location for continental transform faults because plate boundaries typically localize within the continental lithosphere, which is weaker. Because the COB is a boundary between materials of contrasting elastic properties, once a fault is established there, it will probably remain stable. We propose that deformation progressively shifted to the COB in the wake of Yakutat terrane's northward motion along the margin. Minor convergence across the plate boundary is probably accommodated by fault reactivation on Pacific crust and by an eastward dipping QCF. Underthrusting of Pacific slab under Haida Gwaii occurs at convergence angles >14°–15° and may have been responsible for the emergence of the archipelago. The calculated slab entry dip (5°–8°) suggests that the slab probably does not extend into the asthenosphere. The PA/NA plate boundary at the QCF can serve as a structurally simple site to investigate the impact of rheology and composition on crustal deformation and the initiation of slab underthrusting.

Plain Language Summary The Pacific-North America plate boundary offshore British Columbia and Alaska is similar in its length, relative motion, and kinematic history to the plate boundary in California, yet the deformation styles along these plate boundaries are distinct. The California boundary shows a broad zone of parallel strike slip and thrust faults and folds, whereas deformation in Canada and Alaska is centered on a single ~900-km-long fault, the Queen Charlotte Fault (QCF). We propose that the plate boundary along the QCF follows the ocean-continent boundary, an unusual location for continental transform plate boundaries. We propose a scenario for the transfer of plate boundary deformation to the ocean-continent boundary following the passage of a thick oceanic crustal block along the plate boundary. We argue that the contrast in rock properties between oceanic and continental crusts explains the narrow plate boundary. Tectonic deformation due to slight convergence component between the plates is also different than in California. Pacific slab slides under North America along the southern portion of the plate boundary, probably lifting Haida Gwaii archipelago. Convergence farther north may be accommodated by thrust faults on the oceanic crust, by a dipping trace of the QCF, and by minor relative continental block motion.

1. Introduction

Many strike-slip plate boundaries (e.g., San Andreas, Dead Sea, Northern Anatolia, Alpine, Septentrional, and Enriquillo faults) and fault systems accommodating the strike-slip component of oblique subduction (e.g., Sumatra-Andaman and the Philippines faults) are located a few tens of kilometers landward of the continent/ocean boundary (COB), leaving narrow continental slivers, which may partially or completely move with the oceanic plate. Variations in the strength of the lithosphere may exert a major control on the location of rifts and strike-slip plate boundaries (Steckler & ten Brink, 1986; Vink et al., 1984). Under a regional stress field, failure is expected to be focused in the location where the integrated strength of the lithosphere reaches a minimum value. Vink et al. (1984) and Steckler and ten Brink (1986) compared the strengths of various continental provinces and oceanic lithosphere of various ages and thickness by integrating the yield strength envelope of the respective lithospheric columns. Most continental provinces were shown to be weaker than most of the adjacent oceanic lithosphere due to the composition and larger thickness of the

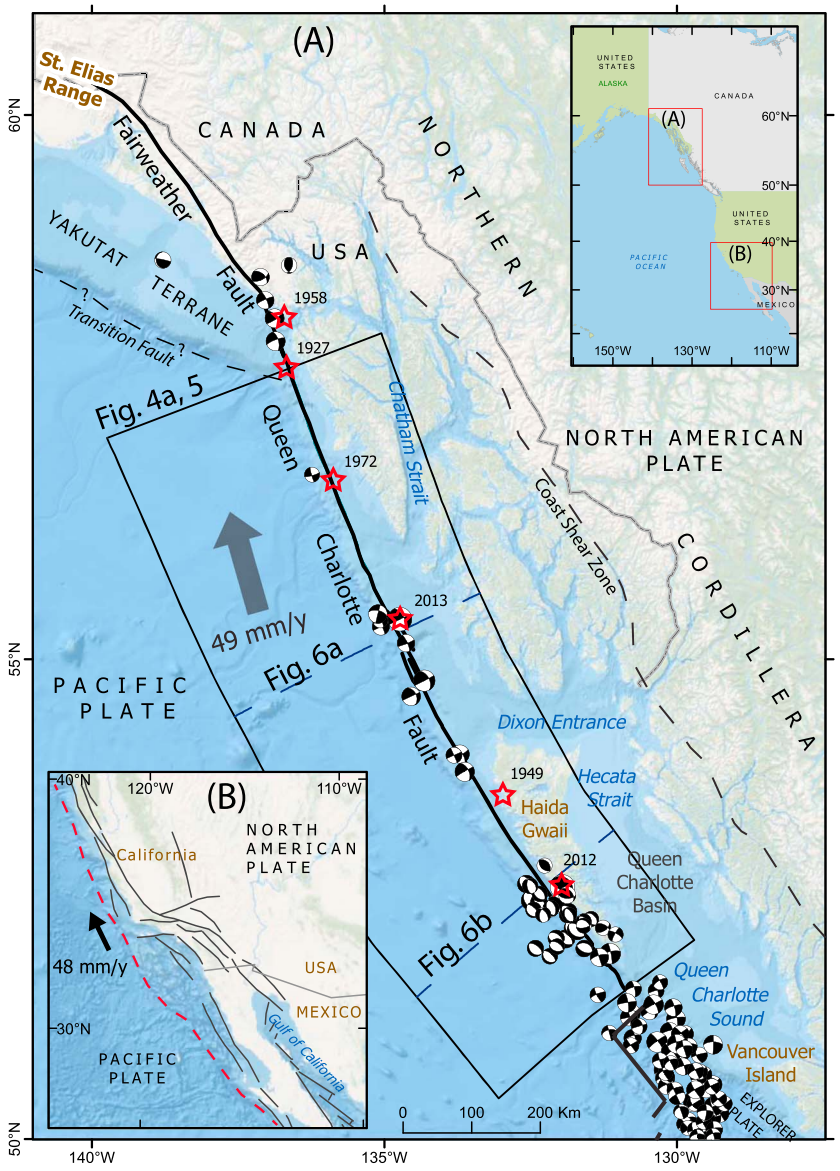

Figure 1. (a) Location map of the study area. Heavy lines—plate boundary faults. Beach balls—earthquake focal mechanisms from the global CMT catalog (http://www.cmt.org., accessed 04/06/2017). The top inset shows location. Red stars—locations of >*M*7 earthquakes along Queen Charlotte and Fairweather faults (www.isc.ac.uk/iscgems, accessed 04/06/2017). (b) Relative plate motion, continent-ocean boundary (red dashed line), and simplified fault map (after https://earthquake.usgs.gov/hazards/qfaults) in California and Baja. Data source—Esri World Ocean Base, USGS. Inset—locations of maps A and B.

continental crust relative to the oceanic crust (Vink et al., 1984) and due to the thermal effect of a thick sedimentary cover, the radiogenic heat production of the continental crust, and sometimes because of the higher thermal gradient due to arc volcanism or slab windows (Steckler & ten Brink, 1986).

An example of a plate boundary following strength minima is the Pacific/North America (PA/NA) plate boundary in California and northern Mexico, where both the rift (Gulf of California) and the strike-slip plate boundary (San Andreas and adjacent faults and Eastern California Shear Zone) are located within the fore arc, arc, and back arc of the former Farallon subduction zone system (Figure 1, inset). The crustal heterogeneity of these continental provinces further dictates the existence of distributed faulting with parallel active strike-slip faults throughout California, as well as intervening thrust faults accommodating a slight compressive component (https://earthquake.usgs.gov/hazards/qfaults). Even with this wide region of distributed faulting, the PA/NA boundary in California and northern Mexico is neither located at the COB nor within the Pacific oceanic plate.

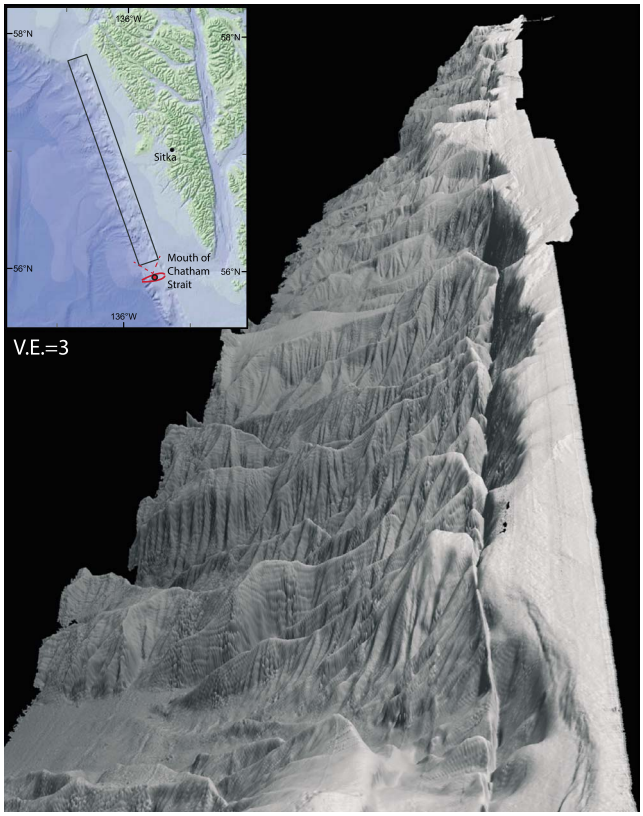

Figure 2. Perspective view of Queen Charlotte Fault looking north from 56°N for 200 km. Shaded bathymetry data after Brothers et al. (2017) gridded at 20-m interval. The rectangle in inset shows extent of hill-shaded perspective view.

The Queen Charlotte-Fairweather fault system is the northern continuation of the PA/NA plate boundary. It extends from the Explorer Triple Junction north of Vancouver Island to the eastern end of the Chugach-St. Elias mountain range, a distance of 1,200 km (Figure 1). As in California, the Alaska-Canada margin experienced a Mesozoic-Early Cenozoic subduction history, followed since about 50 Ma by right-lateral translation. The fault system presently accommodates right-lateral motion of comparable rate to California (48 to 49 mm/yr) with a slight convergence component and is seismically active (six large earthquakes during the past 90 years: 1927 M_s 7.0, 1949 M_s 8.1, 1958 M_s 7.9, 1972 M_w 7.6, 2012 M_w 7.8, and 2013 M_w 7.5; Figure 1). The majority of the plate boundary is located offshore along the 900-km-long Queen Charlotte Fault (QCF). The plate boundary steps on land at Icy Point at its northern end to become the Fairweather Fault. Compared with California, the QCF is unusual because the plate boundary appears to be centered on a single fault located at the edge of the continental shelf along its northern half and at the steep slope (Figure 2) and base of slope in its southern half (Barrie et al., 2013; Brothers et al., 2017; Bruns & Carlson, 1987; Trehu et al., 2015).

The right-lateral Pacific-North America relative motion has a minor component of convergence both in California and in British Columbia and southeast Alaska. Unlike strain partitioning by thrust faults, folds, and block rotations in California, the 2013 M_w 7.5 Craig earthquake along the central QCF (Figure 1) had a strike-slip mechanism on a 75° to 80° inclined fault plane (Yue et al., 2013; https://earthquake.usgs.gov/earthquakes/eventpage/usp000jxum#focal-mechanism—last accessed 6/27/2017). The 2012 M_w 7.8 Haida Gwaii earthquake along the southern QCF, was, on the other hand, a thrust earthquake on a plane dipping to the ENE under the surface trace of the QCF (Kao et al., 2015; Lay et al., 2013). The 2012 Haida Gwaii earthquake was followed by aftershocks located 25 to 40 km seaward of QCF, and focal mechanisms of these events suggest that they were associated with the release of plate bending stresses (Kao et al., 2015). Hyndman and Hamilton (1993), Smith et al. (2003), Bustin et al. (2007), and Hyndman (2015) argued that the convergent component of PA/NA motion in the southern QCF is accommodated by subduction of the Pacific plate under Haida Gwaii by as much as 80 km perpendicular to the plate boundary. In contrast, Rohr et al. (2000) proposed that convergence occurs through distributed deformation and regional crustal thickening on both sides of QCF, in both the oceanic and continental crust. Trehu et al. (2015) suggested that shortening is accommodated within the oceanic crust by the buildup of Queen Charlotte Terrace south of 53.2°N and by short ridges north of this latitude (Trehu et al., 2015).

In this paper, we show that the QCF is located at the COB and propose an evolutionary scenario for the plate boundary, which could explain its anomalous location relative to other transform plate boundaries. We discuss the impact of the location of the plate boundary along the COB on the two components of deformation: along-fault strike-slip motion and the cross-fault convergence. The unique deformation exhibited by the QCF has implications to seismic hazard and perhaps rupture dynamics and raises several questions regarding transpressive deformation and the initiation of plate underthrusting.

2. Background

2.1. Relative Plate Motion History

Oceanic plate subduction since at least 175 Ma (Engebretson et al., 1985) in British Columbia and southeastern Alaska formed an orogenic belt at the western edge of the continent. Slivers of Paleozoic and Mesozoic crustal rocks, known as terranes, have been translated northward as much as hundreds of kilometers along dextral strike-slip faults starting ~100 Myr ago (e.g., Wyld et al., 2006). This northward translation resulted in the juxtaposition of different portions of the orogenic belt and in the formation of the Coast Shear Zone

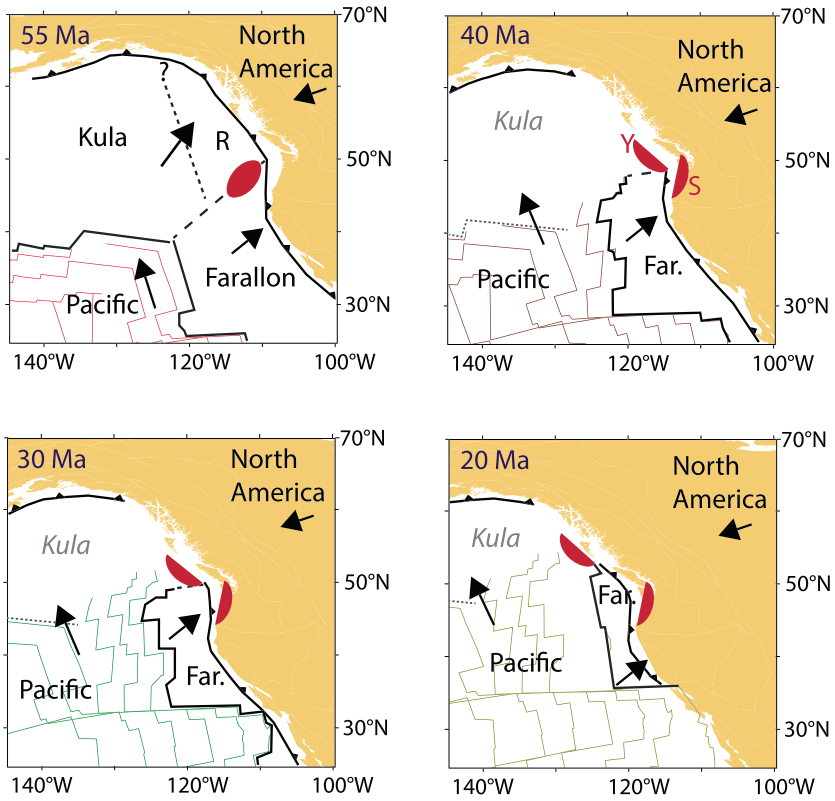

Figure 3. Schematic plate configuration in the East Pacific at 55, 40, 30, and 20 Ma in a fixed reference frame of the Earth spin axis using GPlates (Seton et al., 2012). Colored lines—isochrons on Pacific plate (listed in Seton et al., 2012). Heavy arrows—plate motions relative to the hot spots (after Atwater, 1989). Heavy lines—approximate plate boundaries (dashed where uncertain). Note that Kula plate was captured by the Pacific plate between 55 and 40 Ma and started moving with it to the NNW. The thin dotted line shows extinct plate boundary. Red oval—possible location of the combined Yakutat and Siletz terranes, formed 56–49 Myr ago, perhaps above the Yellowstone hot spot (Wells et al., 2014). The terranes likely straddled the Resurrection-Farallon ridge and subsequently split. Y—Yakutat; S—Siletz; R—Resurrection plate.

(Figure 1; Chardon et al., 1999) and other large fault systems. Subduction continued after the Kula plate separated from the Farallon plate along a spreading ridge 85 to 80 Myr ago and started moving in a more northerly direction (Figure 3; Engebretson et al., 1985; Doubrovine & Tarduno, 2008). The Kula plate may have fragmented, giving rise to a smaller plate, the Resurrection plate, which broke off the Kula plate and was subducting under the margin for at least part of this period (Haeussler et al., 2003). The location of the intersection of the Kula-Farallon spreading ridge (or Resurrection/Farallon ridge) with the continental margin is unknown but was likely in the Washington State and Vancouver Island region (Engebretson et al., 1985; Wells et al., 2014). By about 46 to 40 Ma (or as early as magnetic anomaly 24; 54 Ma, Stock & Molnar, 1988), the Kula plate was captured by the Pacific plate and started moving northward with the Pacific plate, relative to North America (Doubrovine & Tarduno, 2008; Engebretson et al., 1985). This capture and change in relative motion resulted in the cessation of subduction along the British Columbia/Southeastern Alaska margin and the beginning of right-lateral translation. The Pacific/Farallon spreading ridge intersection with the margin remained in the Washington State and Vancouver Island region (Figure 3; Engebretson et al., 1985). Uncertainties in plate reconstruction during this period arise from the absence of a PA/NA spreading center, the complete subduction of the Kula and Resurrection plates, and the disintegration and almost complete subduction of the Farallon plate. PA/NA relative plate motion is better constrained for the past 20 Ma due to a direct contact between the two plates in California, Canada, and Alaska and due to better constraints on the closure of the plate circuit through other plate pairs (e.g., DeMets & Merkouriev, 2016).

The transition from subduction to a right-lateral translation north of the Kula/Resurrection-Farallon ridge intersection with the margin may have created a slab window under the former orogenic belt after 50–40 Ma (Madsen et al., 2006), similar to the configuration of the more-frequently discussed slab window

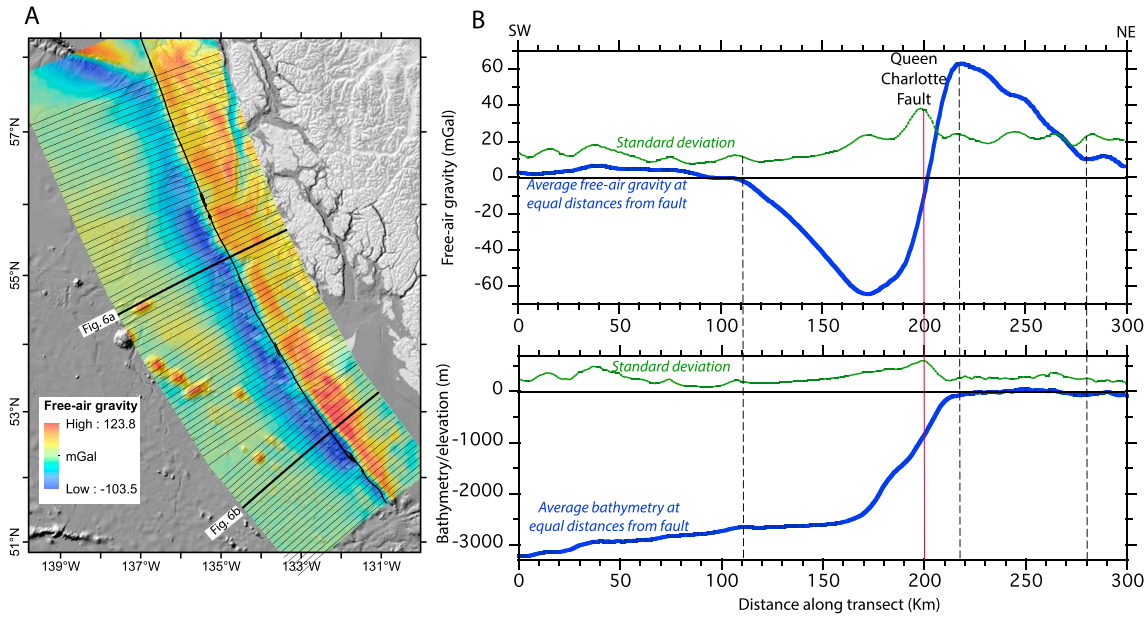

Figure 4. (a) Free-air gravity anomaly map (Sandwell & Smith, v.18.1, accessed 10/16/2016 from www.geomapapp.org). See Figure 1 for locations. Fault-perpendicular lines are locations of gravity and bathymetry spaced 10-km apart. (b) Average gravity and bathymetry of the 79 profiles marked in (a) and their standard deviations. Each profile is sampled at 1-km intervals and extend 200 km seaward and 100 km landward of the fault.

under western California (Dickinson & Snyder, 1979). Ample evidence of postsubduction Cenozoic magmatism within the former fore arc and accretionary prism is explained by the existence of a slab window under the margin (Edwards & Russell, 2000; Madsen et al., 2006).

3. Gravity Data and Modeling

Crustal structure in the vicinity of the QCF is poorly known, except at the latitude of central Haida Gwaii, where offshore and onshore seismic refraction surveys were conducted (Dehler & Clowes, 1988; Horn et al., 1984). Absent seismic and land geology constraints, we use the gravity field to infer the crustal structure across the QCF (Figure 4a). A characteristic gravity profile across the fault was calculated by averaging 79 gravity profiles oriented perpendicular to the fault and spaced 10 km apart (Figure 4b). The profiles extend 200 km seaward and 100 km landward of the fault. The average profile captures the first-order free-air anomaly associated with the fault as evident from the small standard deviation of the difference between individual profiles and the average profile (Figure 4b). To a first approximation the gravity anomaly along the margin is antisymmetric with a steep gradient across the fault and ~60-mGal negative and positive anomalies that taper off at distances of 80–90 km from the fault (Figure 4b).

A residual free-air gravity anomaly (Figure 5a) was constructed by subtracting the average free-air gravity anomaly (Figure 4b) from each of the 79 profiles and gridding the residual profiles. The residual gravity field lacks long wavelength anomalies but shows a change from a positive anomaly to a negative anomaly in the residual free-air gravity along the fault at Lat. 55.4° (Figure 5a). This change reflects the change in water depth of the fault trace from shallow to deep water (as discussed in more detail in section 4.3) and is not associated with crustal variations. This interpretation is confirmed by the absence of changes in Bouguer gravity anomaly at this latitude (Figure 5b). The Bouguer anomaly corrects for differences in water depth.

A linear negative free-air residual anomaly is observed along the fault south of 53.1°N and is coincident with the location of Queen Charlotte Terrace west of Haida Gwaii. The anomaly is negative relative to the anomaly along the fault to the north and to the west, which we attribute to thick, low-density sediments, as discussed below and in section 5.1. Closed short wavelength negative Bouguer gravity anomalies seaward of the fault are interpreted to represent pockets of thick low-density rocks, some underlying shallower seafloor.

Crustal density models were constructed along two gravity and bathymetry profiles crossing the epicenters of the 2013 Craig and 2012 Haida Gwaii earthquakes (Figure 6). These models were kept intentionally

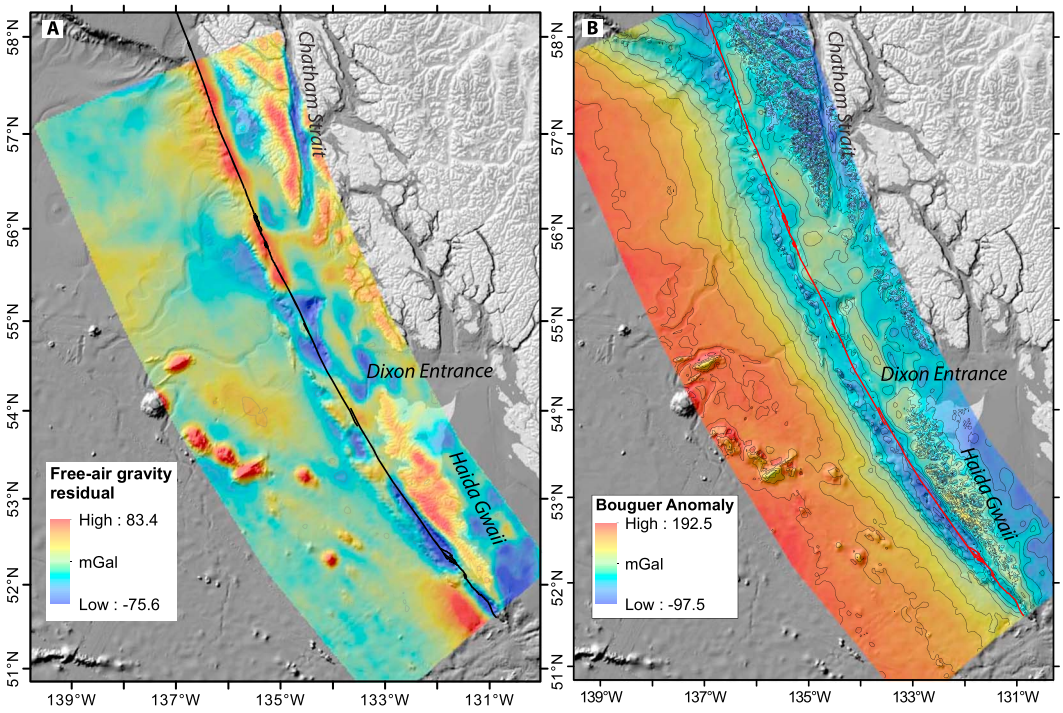

Figure 5. (a) Residual free-air gravity calculated by averaging the 79 profiles shown in Figure 4a as a function of distance from the Queen Charlotte Fault (heavy line) and subtracting the average gravity profile (b). (b) Bouguer gravity anomaly calculated every 1 km along each of the 79 profiles shown in Figure 4a and gridded. Contour interval 20 mGal. Bouguer correction with densities of 2,670 kg/m^3 and 2,200–1,030 kg/m^3 were used above and below sea level, respectively, to account for the exposed crystalline basement above sea level and the mostly late Cenozoic sediment below sea level.

simple having only four density boundaries and by making the upper crust/lower crust density boundary landward of the fault horizontal to minimize its contribution to the gravity anomaly. We assumed a typical 8-km-thick oceanic crust. A thin layer with a density of 2,670 kg/m^3 was added for the parts of the profile above sea level. The modeled Moho depth along the continental side of Figure 6a is 24 km, in agreement with seismic refraction and reflection results in the eastern part of Dixon Entrance (23–25 km, Morozov et al., 2001) and the minimal sedimentary cover on the shelf (Bruns & Carlson, 1987; Gehrels & Saleeby, 1987). This Moho depth is also consistent with the fault dip of the 2013 Craig earthquake (Lay et al., 2013, https://earthquake.usgs.gov/earthquakes/eventpage/usp000jxum#focal-mechanism). The modeled Moho depth along the Haida Gwaii profile (Figure 6b) is 27 km, in agreement with Moho depth determined by seismic refraction under Queen Charlotte Basin (Spence & Asudeh, 1993).

The sediment-crust interface in our model for Haida Gwaii follows the rupture surface and aftershocks of the 2012 earthquake (Figure 6b) and is similar to Yuan et al. (1992) model for a profile south of Haida Gwaii. Furthermore, despite the relatively shallow water of Queen Charlotte Terrace, the terrace is associated with a negative residual free-air gravity anomaly (Figure 5a). The negative residual anomaly indicates the presence of low-density sediment filling of the space formed by the down-flexed oceanic crust. The top of the dipping oceanic crust under the QCF trace in our model (Figure 6b) is at 12.25 km, similar to the depth of 12.75 km in a rupture model for the 2012 Haida Gwaii earthquake (Lay et al., 2013). We opted to ignore published velocity models of Queen Charlotte Terrace (Dehler & Clowes, 1988; Horn et al., 1984), which show narrow vertical blocks extending throughout the sediment and crust. These blocks have horizontally varying velocities, which are much lower than the adjacent oceanic and continental crusts. This blocky velocity structure was based on sparse refraction data and was constructed by merging models for individual shot or receiver gathers (Dehler & Clowes, 1988; Horn et al., 1984). Subsequent gravity models of the blocky structure (e.g., Rohr et al., 2000) used ad-hoc densities to fit the observations rather than published velocity-density relationships. Most important, this complex blocky structure is inconsistent with the underthrust geometry required by the 2012 Haida Gwaii main shock and aftershocks (see Figure 8 of Hyndman, 2015).

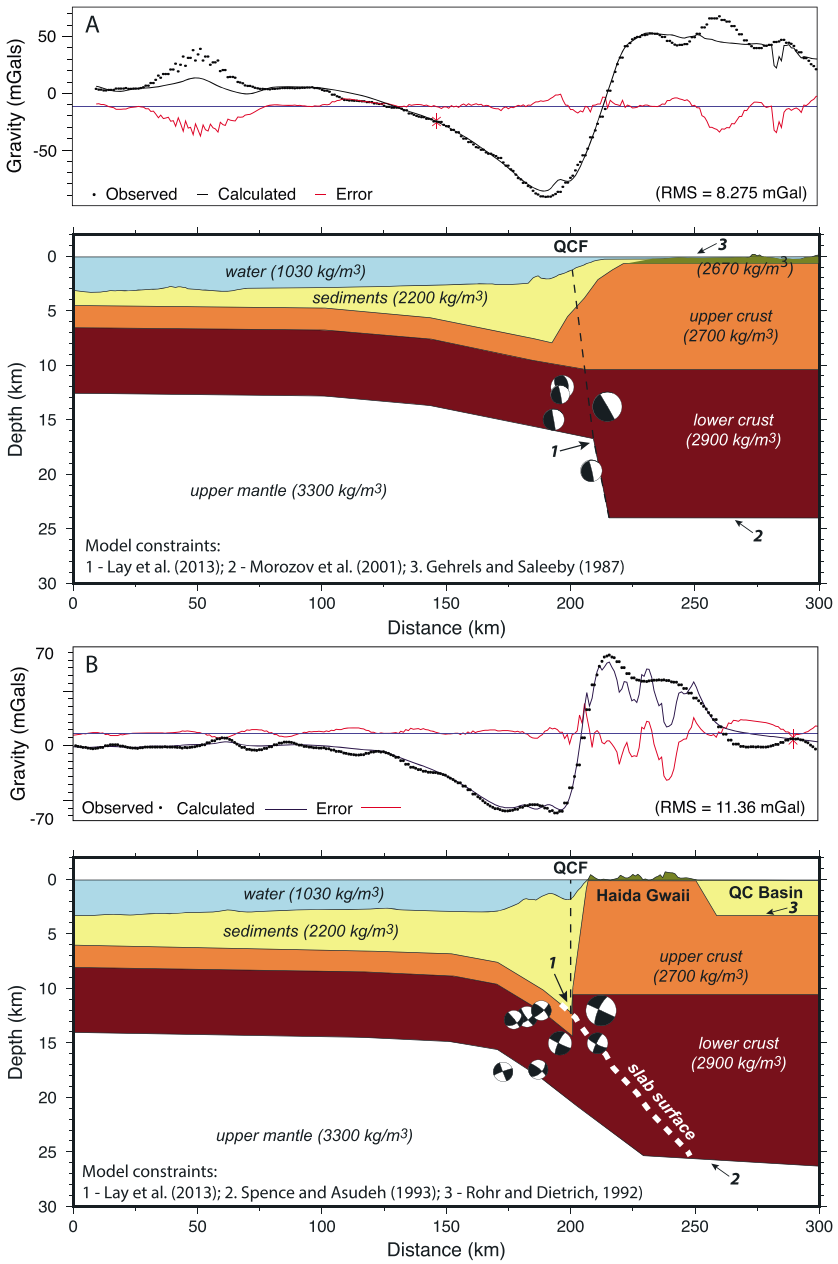

Figure 6. Gravity profiles perpendicular to Queen Charlotte Fault at the location of (a) 2013 Craig earthquake and (b) 2012 Haida Gwaii earthquake. Beach balls—cross-sectional view of earthquakes focal mechanisms from the Global CMT catalog (http://www.cmt.org., accessed 04/06/2017) within 20 km of the profiles. The gravity models include only four layers, and the upper/lower crustal boundary is horizontal to minimize the free model parameters.

4. Plate Boundary at the Continent-Ocean Boundary

4.1. Interpretation Based on Gravity

An antisymmetric gravity anomaly as seen along the QCF (Figure 4b) is typical of the gravity edge effect that arises from summing two gravity step functions with opposing polarity and with different wavelengths. A negative anomaly of a shorter wavelength on the seaward side of the fault arises from the shallow density contrast between basement on the landward side and air/water/sediment on the seaward side. A positive anomaly of a longer wavelength on the seaward side of the fault arises from the shallower upper mantle on the seaward side than on the landward side because of isostatic balance. Summing these opposing anomalies with different wavelengths results in an antisymmetric edge effect anomaly.

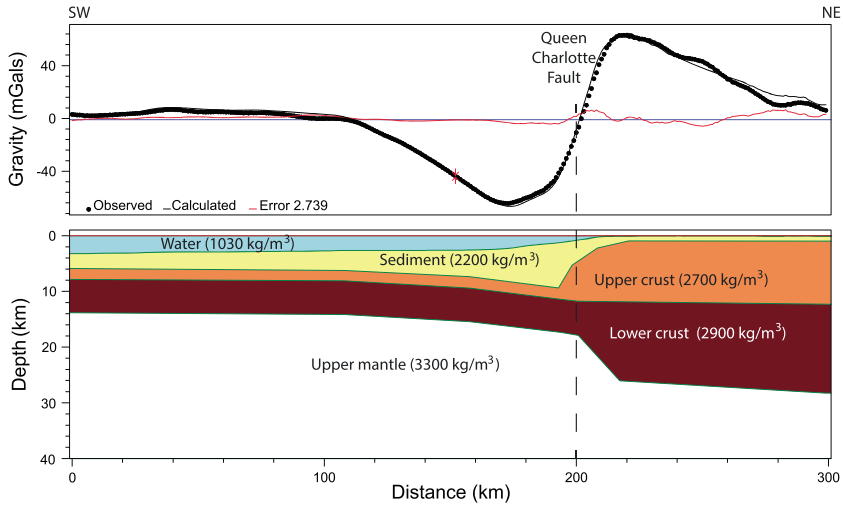

Figure 7. Gravity model of the average gravity and bathymetry profiles shown in Figure 4b. An 8-km-thick ocean crust and a simple four-layer continental crust with horizontal density boundaries were used to minimize the number of free parameters.

A simple five-layer gravity model (Figure 7) reflects the qualitative interpretation of the first-order free-air gravity field and shows that the average gravity anomaly across the QCF can arise from the juxtaposition of crusts with different thickness across the fault. The modeled transition from oceanic to continental crust starts at the fault and extends horizontally landward $<$20 km. The oceanic crust in our model is slightly bowed down toward the fault to produce the slightly longer wavelength of the negative anomaly seaward of the fault relative to the positive anomaly landward of the fault. The gravity field, therefore, suggests that the QCF is located at the COB.

4.2. Stability of the Plate Boundary at the COB

If the QCF is located on the COB, then the QCF separates continental from oceanic crusts, which have different elastic properties. Quantitative analysis of Mode II rupture (shear) along an interface between blocks with different elastic properties (i.e., bimaterial rupture) has shown a dynamic reduction in normal stress, which decreases the effective frictional strength of the fault and facilitates further rupture propagation along the interface (Weertman, 1980; Ben-Zion, 2001). Numerical experiments by Brietzke and Ben-Zion (2006) have shown that slip generally tends to migrate from faults embedded in uniform material toward faults that are located along the material interface. Therefore, once a fault is established along the bimaterial interface, its location is expected to remain stable and does not easily migrate laterally to one crust type or the other.

Once established, the stability of the plate boundary at the COB may also be aided by deviatoric tensile stresses across the edge of the continental crust. Sharp thickness and elevation differences across the COB lead to buoyancy contrasts at each level of the crust. This contrast may cause tensile stresses of $\leq$40 MPa for a lateral density contrast of 50 kg/m^3 between North American upper crust and the 8-km-thick water and sediment overlying the Pacific plate and assuming lithostatic conditions.

Based on the models referenced above, rupture should take place along a single fault on the COB (the QCF) and not along several parallel fault strands distributed in the continental crust. The location of the fault trace is expected to remain stable over many earthquake cycles, and a single fault trace would be expected to accommodate the entire relative plate motion. Analysis of offsets of glacio-fluvial features along the fault trace, mapped with multibeam bathymetry, shows a cumulative offset which is commensurate with the total offset since LGM (Brothers et al., 2017; Greene et al., 2016). For example, three fault-crossing submarine canyons were successfully restored (Figures 8b and 8c) by reversing the expected 833-m fault offset since the collapse of the ice cap in southeastern Alaska ~17,000 years ago (Brothers et al., 2017) with the predicted PA/NA relative motion of 49 mm/yr (DeMets & Merkouriev, 2016). The underlying assumption of this restoration is that the seafloor was largely reset and smoothed by sediment input during the ice cap collapse.

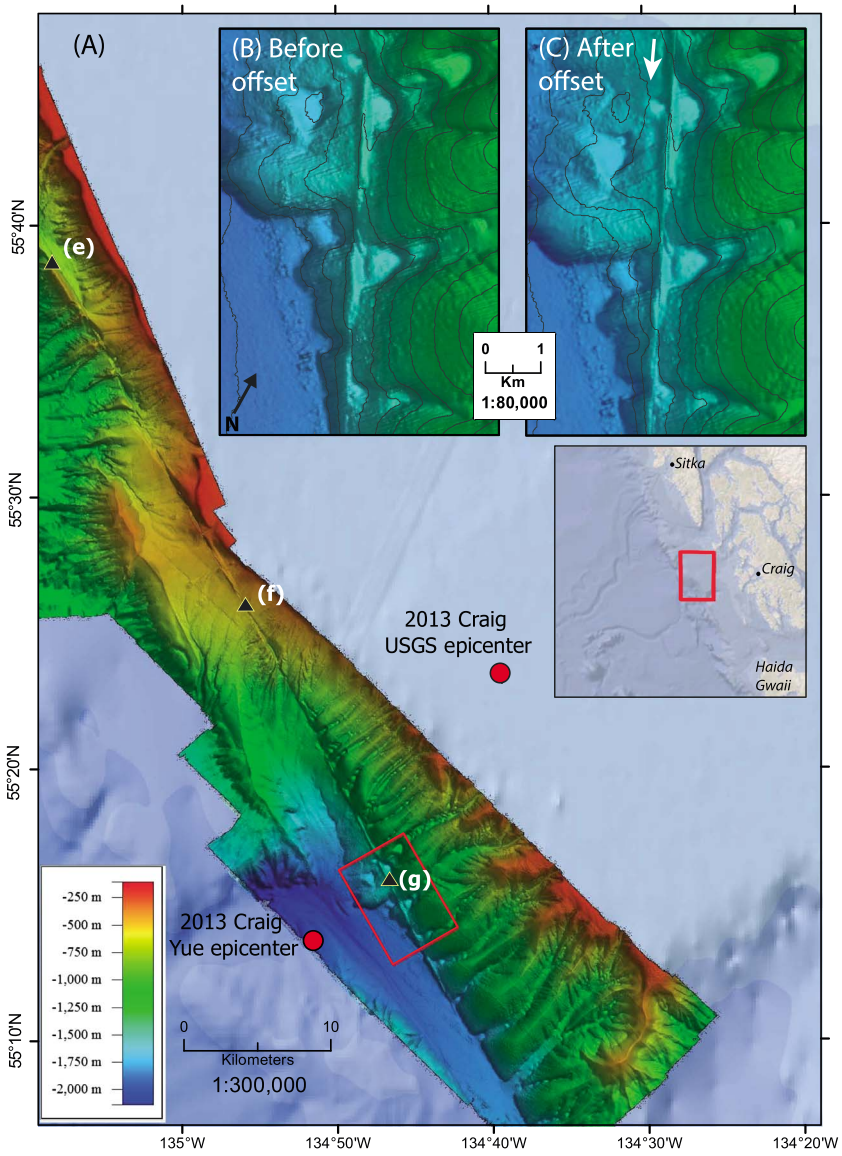

Figure 8. (a) Multibeam bathymetry map of a segment of Queen Charlotte Fault offshore Craig, Alaska (after Brothers et al., 2017) at the location where the fault descends from the shelf edge to the lower slope. See inset for location. (e–g) Locations of profiles in Figure 13. Red dots: locations of 2013 Craig earthquake epicenter from U.S. Geological Survey (https://earthquake.usgs.gov/earthquakes/eventpage/usp000jxum#focal-mechanism) and Yue et al. (2013). Red rectangle—location of (b) and (c). (b and c) Enlargement of a segment of the fault before and after applying an offset of 833 m to reverse the predicted right-lateral relative plate motion since 17,000 years ago. Contour interval 100 m. Note the alignment of the three submarine canyons after the offset.

4.3. Margin Morphology Does Not Follow the COB

The QCF trace runs along the shelf edge at its northern end for about 350 km (Brothers et al., 2017; Figure 2), before cutting diagonally across the slope and continuing southward in ~2,000-m deep water at 55.4°N (Figure 8a). South of ~54.3°N and offshore Haida Gwaii, the fault trace alternates between shallow, intermediate, and deep water, cutting across local westward extensions of the shelf and Queen Charlotte terrace (Barrie et al., 2013; Bruns et al., 1992).

We suggest that the position of the fault with respect to the shelf edge is simply the result of the north-to-south increase in the distance from the terrestrial and glacial sediment supply source. The extent of the Late Wisconsin ice cap in southeastern Alaska generally overlaps its mountainous region with major ice streams reaching the shelf edge (Molnia, 1986; Powell & Molnia, 1989; Kaufman & Manley, 2004). The distance from the mountainous region to the fault increases from north to south. An ice cap did not exist on Haida

Gwaii and the surrounding continental shelf except for small alpine glaciers on the islands, and these mountain glaciers mostly drained eastward toward Hecate Strait. The main ice cap in this sector of British Columbia was located east of Hecate Strait (Hetherington & Barrie, 2004). A possible LGM ice sheet in Dixon Entrance had drained to the NW where it probably coalesced with ice lobes from southern Alaska (Lyles et al., 2017). Thus, only in the northern sector was sediment supply sufficiently large to prograde and build a shallow-water shelf all the way to the QCF (Figure 2).

4.4. Why Did the Plate Boundary Form at the COB?

The location of the PA/NA plate boundary along the COB is unusual when compared to the plate boundary farther south in California and to other strike-slip plate boundaries. Parts of the former arc and fore arc of the North America plate are expected to constitute the weakest lithosphere within the PA/NA margin, focusing the relative plate motion in these regions. In this section, we propose a scenario where deformation within the fore arc and arc had shut off progressively from south to north as Yakutat terrane was translating northward along the margin establishing the QCF in its wake (Figure 9, inset).

The Yakutat terrane is a block of thick crust underlying the eastern and central part of the Gulf of Alaska (e.g., Worthington et al., 2012) and extending northwestward under southern Alaska as far north perhaps as the central Denali Fault (Ferris et al., 2003; Eberhart-Phillips et al., 2006). The Yakutat is presently thrust under the Chugach-St. Elias Ranges (Figure 9), uplifting the range since probably 5–6 Ma (Eyles & Lagoe, 1998). Northward translation of the Yakutat terrane provides an explanation for the 50 to 55-Ma-old basaltic crust of the Yakutat terrane and the more southerly origin of the faunal assemblage and paleosols found within the overlying sediments (Bruns, 1983; White et al., 2017). Wells et al. (2014) proposed that the Yakutat terrane formed 55–49 Myr ago concurrently with the Siletz Terrane, which underlies coastal Washington and Oregon, as a large igneous province straddling the Kula-Farallon or Resurrection-Farallon Ridge (Figure 3). Our reconstruction of Yakutat terrane, based on PA/NA stage poles of DeMets and Merkouriev (2016) for the past 20 Ma and Doubrovine and Tarduno (2008) for the earlier period, supports this interpretation (Figure 9).

To quantitatively identify the location of the weakest lithosphere across the margin, we calculated the integrated strength (e.g., Steckler & ten Brink, 1986) of the Kula oceanic lithosphere, the continental lithosphere, and the Yakutat terrane. The strength of the lithosphere was calculated by integrating the failure stress under the yield strength envelope (Figures 10b and 10c). A strength comparison between the different lithospheres was calculated for the region at 20 Ma, the earliest available confident stage pole (DeMets & Merkouriev, 2016). The Yakutat terrane was then located off the southern end of Haida Gwaii (Figure 1). Because the Yakutat terrane formed ~53 Ma on the Resurrection-Farralon or Kula-Farallon ridge (Wells et al., 2014), the seafloor age north of the Yakutat terrane 20 Myr ago had to be older than 33 Ma.

We assumed an 8-km-thick oceanic crust with diabase composition (Mackwell et al., 1998) and either wet or dry olivine composition of the oceanic mantle (Hirth & Kohlstedt, 2003). For the continental lithosphere, we used a 30-km-thick crust of the late Cretaceous to Eocene former arc (Morozov et al., 2001), the youngest subduction-related crust along the margin with wet anorthosite composition (Rybacki & Dresen, 2000) and dry olivine for the mantle. For the Yakutat terrane, we used a 30-km-thick crust (Worthington et al., 2012) with diabase composition (Mackwell et al., 1998) and dry olivine for the mantle.

The ductile failure stress is highly dependent on the lithospheric geotherm (Figure 10a). To calculate the continental geotherm, we set the surface heat flow $Q_0 = 73 \pm 11$ mW/m^3 and radiogenic heat production $A_0 = 1.6 \pm 0.8\text{e}{-6}$ W/m^3 for the Northern Cordillera (Lewis et al., 2003). We used typical values for surface temperature of 0 °C and a logarithmic decrement of radiogenic heat production (Lachenbruch, 1970) with thermal conductivity $K = 2.5$ W/(m-K), thermal diffusivity $\kappa = 1\text{e}{-6}$ m^2/s, a skin depth DHF = 15 km, and a basal heat flux of $A_0 \times$ DHF. The geotherm of the oceanic lithosphere (Figure 10a) assumes a normal asthenosphere temperature of 1,300 °C at an age-dependent depth, calculated using the half-space cooling model for a 33-Ma oceanic lithosphere minus its age-dependent water depth. To calculate a minimum strength estimate for the Yakutat terrane, we modeled the Yakutat as an oceanic plateau formed by a hot spot with an extremely high mantle temperature of 1,500 °C (McKenzie & Bickle, 1988).

The yield strength envelope (Figure 10b) was calculated by choosing the smallest of brittle failure stress for strike-slip faulting (Ranalli, 1995) and the ductile failure stress. Stress slopes of the brittle failure with depth for

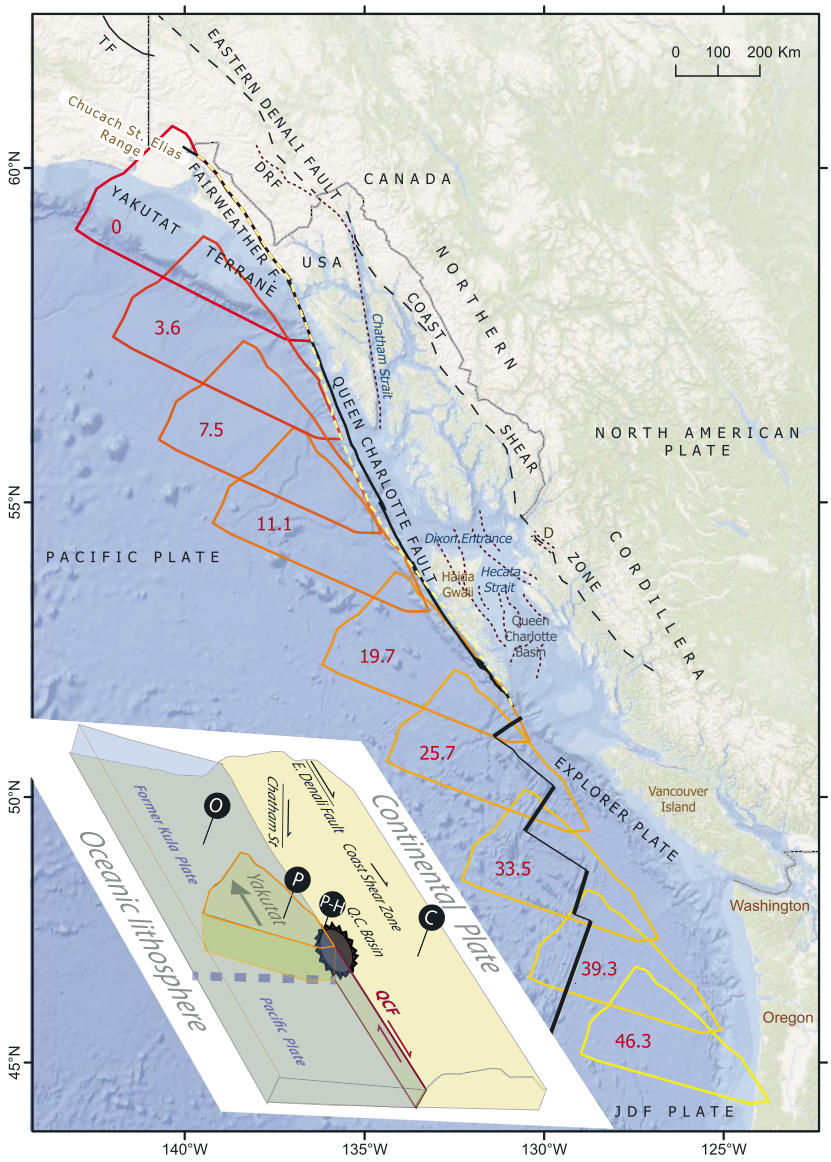

Figure 9. Yellow to red polygons—Yakutat terrane location for selected stage poles with their corresponding age in Myr using the stage poles of DeMets and Merkouriev (2016) for ages<20 Ma and Doubrovine and Tarduno (2008) for ages >20 M. The outline of the present Yakutat terrane encompasses crustal thickness > 20 km (Worthington et al., 2012). Yellow dashed line—trajectory of Yakutat terrane during the past 20 Ma using DeMets and Merkouriev (2016) stage poles. Dashed brown lines—Late Cenozoic transtensional and strike-slip faults discussed in the text which are no longer active or are dying. DRF—Duke River fault; D—location of Cenozoic strike-slip activity from Davidson et al. (2003). Faults under Hecate Strait are from Hollister et al. (2008), but their delineation is uncertain due to sparse data coverage. TF—Totschunda Fault; JDF—Juan de-Fuca. Inset—schematic representation of the configuration of the plate boundary ca. 20 Ma when the thick part of Yakutat terrane was located at the southern end of Haida Gwaii. C—continent; O—oceanic lithosphere; P—oceanic plateau; P-H—oceanic plateau heated; Q.C. Basin—Queen Charlotte basin.

crustal pore fluid pressures, λ, of 0 and 0.7 (dry and ≫ hydrostatic; Brace & Kohlstedt, 1980) are 32.1 and 9.6 MPa/km, respectively, assuming friction coefficient μ = 0.7 and a crustal density of 2,800 kg/m^3. Ductile stress failure was calculated using strain, composition, and a temperature-dependent flow law for dislocation creep (Table 1). A typical strain rate of 1e−14 s^{-1} was chosen, and the above-discussed geotherms were used for the continental, oceanic, and Yakutat oceanic plateau lithospheres.

Despite the assumed high mantle temperature of Yakutat terrane, the continental lithosphere is weaker than the oceanic lithosphere and the Yakutat terrane (Figure 10c). One way of shifting the location of the weakest lithosphere to the COB is by reducing the integrated strength of the Yakutat terrane via heating. Heating does not have to be significant: Increasing the geotherm to the equivalent of a 22 and 9-Ma oceanic lithosphere

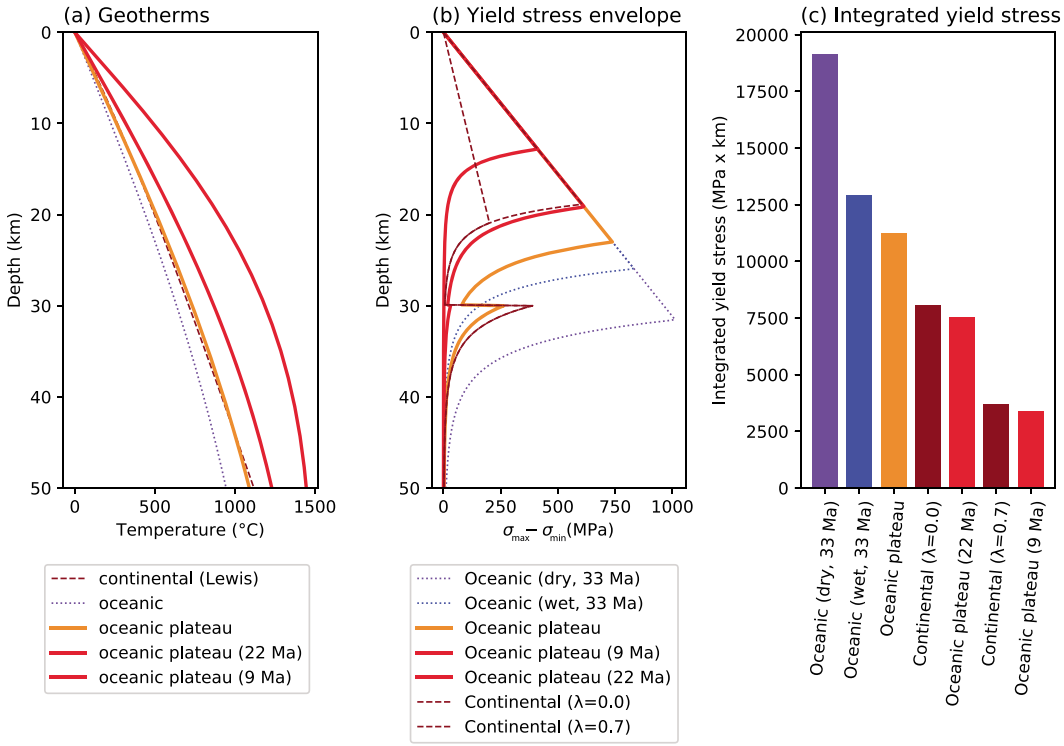

Figure 10. (a) Geothermal gradients for continental lithosphere, Kula oceanic lithosphere with an age of 33 Ma, Yakutat oceanic plateau with an age of 33 Ma, and Yakutat oceanic plateau heated to oceanic geotherms equivalent to 22 and 9 Ma. Temperature at base of oceanic lithosphere is assumed to be 1,300 °C and at base of oceanic plateau at 1,500 °C in order to lower the strength of oceanic plateau. (b) Yield strength envelopes at t = 20 Myr ago for the oceanic lithosphere and the Yakutat oceanic plateau and for the continental lithosphere with a friction coefficient μ = 0.7 and pore fluid pressures, λ = 0 and λ = 0.7. Also shown is the yield strength envelope for the Yakutat oceanic plateau heated to geotherm ages of 22 and 9 Ma to lower its strength below that of the respective continental lithosphere. (c) Integrated lithospheric strength at t = 20 Myr ago for the yield strength envelopes in (b).

will lower its integrated stress to below that of dry and "wet" continental lithosphere, respectively (Figure 10). A possible heating mechanism for the Yakutat terrane is the proximity of a young and hot Pacific lithosphere to the southern edge of the Yakutat terrane ~20 Myr ago (Figure 9, inset). The region south of the Yakutat terrane is Pacific oceanic crust formed at the Pacific-Farallon ridge. Because the ridge-margin intersection had remained stable along the Vancouver Island-Washington coast (Figure 3), the age of Pacific crust was likely very young during at least part of the period, progressively warming the southern edge of the Yakutat terrane as it migrated northward (Figure 9).

4.5. Propagation Model for the Plate Boundary

Based on strength arguments (Figure 10), we hypothesize that past PA/NA relative plate motion has been distributed among several faults within the former arc and fore arc, similar to California. The heating of the thick Yakutat crust may have ultimately made the lithosphere there weaker than the continental lithosphere and, combined with possible focusing of the deformation at the rheological boundary (section 4.2 above), may have allowed the plate boundary to shift to the continental edge. As the Yakutat terrane migrated northward, the QCF propagated northward with it along the bimaterial boundary, transferring the locus of interplate strike-slip motion from the former arc and fore arc to the COB (Figure 9, inset).

Documenting late Cenozoic displacement within the arc and fore arc is hampered by the paucity of Neogene rock units that can serve as markers of such strain. Nevertheless, there is evidence for late Cenozoic deformation within the former arc and fore arc. Seismic and well data from Queen Charlotte basin underlying Hecate Strait and eastern Dixon Entrance show >20-Myr-old mixed extension and

Table 1
Parameters of Dislocation Creep Used for Yield Strength Calculation

	A (MPa^{-n}/s)	n	Qp (kJ/mole)	Reference
Dry olivine	110,000	3.5	530	Hirth and Kohlstedt (2003)
Wet olivine	806,130[a]	3.5	480	Hirth and Kohlstedt (2003)
Columbia Diabase	190	4.7	485	Mackwell et al. (1998)
Wet anorthosite	398	3	356	Rybacki and Dresen (2000)

[a]Calculated using $a = \alpha(C_{OH})^r$ where fugacity C_{OH} = 5,000 H/106 Si and the constants r = 1.2, and α = 30 (Miller & Behn, 2012).

strike-slip faulting (Figure 9; Hyndman & Hamilton, 1993; Hollister et al., 2008; Rohr & Dietrich, 1992). Concurrent volcanic and magmatic activity on Haida Gwaii mostly ended 19 Myr ago (Hyndman & Hamilton, 1993). Some dextral strike-slip activity was documented along the Coast Shear Zone around ~30 Ma (D in Figure 9; Davidson et al., 2003). The previous explanation for the cessation of the magmatic activity invoked a change in relative plate boundary from a slight extension to pure strike slip (Hyndman & Hamilton, 1993), yet plate reconstruction shows extension at Haida Gwaii at stage poles corresponding to 11–16 Ma and 18.1–18.7 Ma (Figure 10). We attribute the cessation of transtensional deformation and magmatic activity to the passage of Yakutat terrane and the migration of the deformation to the COB. Farther north, 27 to 25-Ma basaltic rocks across Chatham Strait appear offset by 100 km (Hudson et al., 1982), and marine geophysical data cannot resolve evidence for motion along the Chatham Strait fault or the northernmost Coast Shear Zone since ~13 ka (Brothers et al., 2018). The Duke River fault, which runs parallel to the southern section of eastern Denali Fault (Figure 9), became inactive during the late Miocene (Cobbett et al., 2016; Trop et al., 2012). Richter and Matson (1971), Elliott et al. (2010), and Brothers et al. (2018) have suggested that a northward extension of Fairweather Fault into Totschunda Fault (see Figure 9 for location) is progressively replacing the motion on Eastern Denali fault.

5. Accommodation of the Shortening Component

Although the PA/NA relative plate motion has a small component of convergence in both California and in Canada-southeastern Alaska, the accommodation styles of this shortening are very different between the two regions. Moreover, there seems to be at least two different accommodation styles along the QCF as is evident by the different focal mechanisms of the 2012 M_w 7.8 Haida Gwaii thrust and the 2013 M_w 7.5 Craig strike-slip earthquakes.

Relative plate motion along QCF has changed during the past 20 Ma from divergence and pure strike slip to convergence (DeMets & Merkouriev, 2016). Hyndman (2015) suggested that, prior to 6 Ma, divergence was accommodated by counter clockwise rotation of Yakutat terrane. However, most of this pre-6-Ma divergence occurred north of the intersection between QCF and Yakutat terrane (Figure 11e), which, according to our model, was on the now-subducted Kula plate (see Figure 9, inset), where the QCF had not yet existed. Slight divergence ($\leq$2°) on the QCF is only predicted by DeMets and Merkouriev (2016) stage poles during 9.1–14.6 Ma, when the Yakutat-QCF intersection (Figure 9) was at ~52° to 53.5°N (Figure 11e). Convergence started at the southern end of the fault at ~11 Ma and spread northward as the relative plate motion became more oblique. By 5.2 Ma, the entire QCF experienced either convergence or pure strike slip. The present convergence angle varies gradually from 4° in the north to 22° in the south (Figure 11e).

5.1. Underthrusting South of ~53.1°N

The 2012 M_w 7.8 Haida Gwaii earthquake epicenter and focal mechanism (Lay et al., 2013) lend support to Hyndman's (2015, and references therein) hypothesis that the Pacific plate is subducting under the southern QCF at Haida Gwaii. To better understand the consequences of this hypothesis, we calculated the trajectory of the Pacific slab under the North American margin. We assumed that underthrusting only happens when the convergence angle exceeds a minimum value (e.g., 10°, 15°, or 20°, Figure 11f). We further assumed that the location of the fault trace did not change with time, because the trace of the northward migration of the Yakutat terrane is very similar to the trace of the fault (Figure 9). Trajectories were calculated using DeMets and Merkouriev's (2016) stage poles for points spaced at 10-km intervals along the fault trace. Underthrusting at angles $>$10° predicts that underthrusting could have started as early as 9 Myr ago (Figure 11e) and that a Pacific slab is present under North America almost to the Craig earthquake epicenter (Figure 11f). If underthrusting only occurred at angles $>$20°, a slab is predicted to underlie only the southernmost end of Haida Gwaii (Figure 11f) and could have started only 3 Myr ago (Figure 11e). Underthrusting at convergence angles $\geq$15° predicts that underthrusting could have started 6 Myr ago (Figure 11e) and that the slab extent overlaps almost exactly the land area of Haida Gwaii above the 100-m contour (Figures 11f and 12). The west coast of Haida Gwaii follows the azimuth of the QCF to the location of the present convergence angle of 15° and then departs from the fault in a more northerly orientation, as predicted by the kinematic model. The predicted slab does not extend into Dixon Entrance. A minimum convergence angle of 15° was suggested by Trehu et al. (2015) for the creation of the accretionary prism of the Queen Charlotte Terrace (see Figure 12 for location) on the Pacific side of QCF.

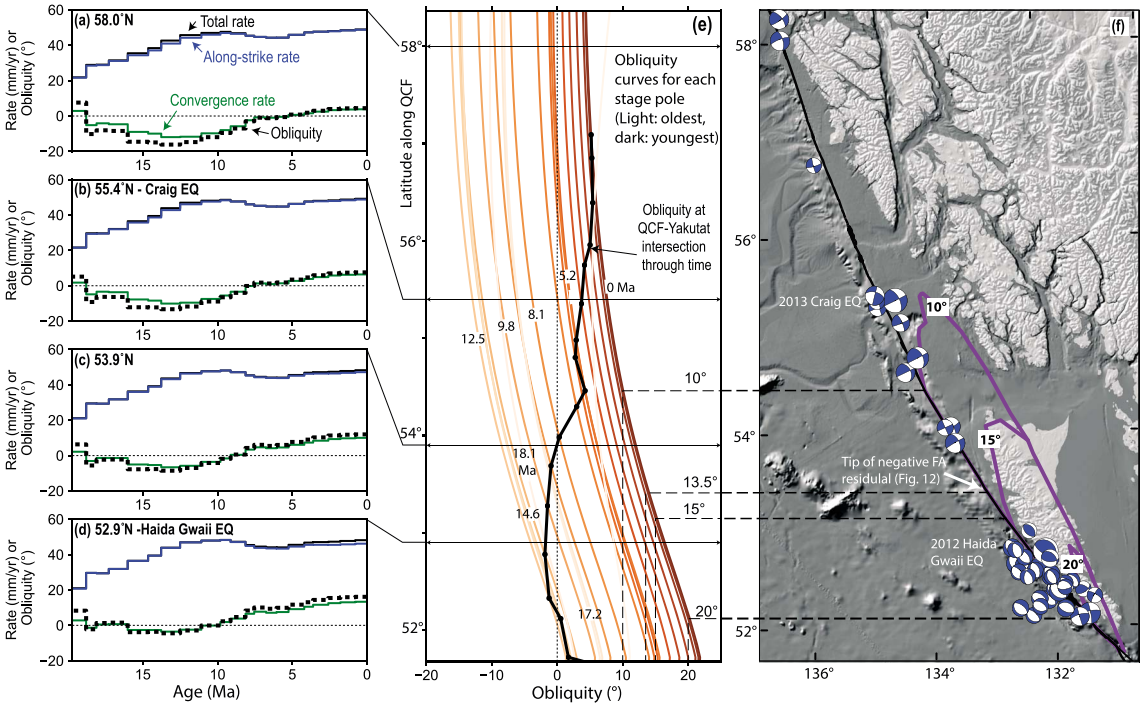

Figure 11. (a–d) Total relative Pacific/North America (PA/NA) rate of motion through time, its component parallel (strike-slip rate) and perpendicular (convergence rate), and angle of obliquity, in four locations along the Queen Charlotte Fault (QCF). (e) Colored curves—obliquity along the fault for different ages using DeMets and Merkouriev (2016) "reduced-noise" stage poles for PA/NA motion during the past 20 Ma. The colors grade according to age with lightest being oldest and darkest being youngest. Black curve—obliquity with time of the QCF/Yakutat intersection located at the SE corner of Yakutat terrane (Figure 9). Time can be read from the black curve's crossings (dots) with the colored obliquity curves of different ages. Between 8 and 14 Ma the QCF/Yakutat intersection was under extension with $<2°$ obliquity and, for the remaining history, was under compression. (f) Predicted extent of underthrusted Pacific slab, assuming that underthrusting occurs whenever the convergence angle is $>20°$, >15, or $>10°$. The horizontal dashed lines connect the predicted present obliquity angle to their respective locations along the fault. The vertical dashed lines intersect the obliquity curves and show the period and the fault segment in which obliquity was higher than 10°, 15°, and 20°. The dashed line for 13.5° denotes the location of the northern tip of residual free-air gravity anomaly which may mark the northern end of underthrusting (see text for further discussion). Beach balls—earthquake focal mechanisms (similar to Figure 1).

The northward end of the strong negative residual free-air gravity anomaly suggests that the initiation of underthrusting may start at a slightly lower convergence angle ($<14°$) and extend farther north to 52.25°N (Figures 11f and 12). A strong negative residual anomaly indicates that the oceanic crust seaward of the fault is depressed, likely because of downward bending. This is despite the shallower topography of Queen Charlotte Terrace, which contributes a positive free-air anomaly. The focal mechanisms of smaller earthquakes along the fault also show a distinct change from thrust and normal fault plane solutions south of 53.0° to 53.5°N to strike-slip solutions farther north (Figure 11f), as was previously noted by Ristau et al. (2007).

Davis and Riddihough (1982), Rohr and Furlong (1995), and Hyndman (2015) suggested that prior to ~6 Ma, the QCF extended to northern Vancouver Island, but plate reorganization transferred Winona basin (Figure 12, inset) to Explorer plate and the QCF retreated northward to its present position. Because convergence angle increases to the south, underthrusting is expected to have started earlier in this segment. Figure 12 (inset) shows the predicted underthrusted oceanic lithosphere beneath North America, assuming a minimum convergence angle of 15°. The underthrusting region reaches a maximum width of 53 km and slightly overlaps with the southernmost Haida Gwaii. Yuan et al. (1992) identified a reflector dipping 9° beneath the outer shelf and modeled a single unreversed refraction and coincident gravity profile with a slab dip of ~14°. A better definition of the underthrusting geometry may help shed light on the evolving geometry of Explorer plate.

Assuming that the focal plane of the 2012 M_w 7.8 Haida Gwaii earthquake defines the dip of the slab interface, and knowing the slab trajectory, we can calculate the dip angle at which the slab enters under the QCF. The entry dip along the slab trajectory, $\Psi_1 = \tan^{-1}(\sin\theta \tan\Psi_2)$, where θ is the angle of oblique convergence (0° is no convergence) and Ψ_2 is the slab dip measured from focal plane solution. Using the focal plane dip of 18.5°

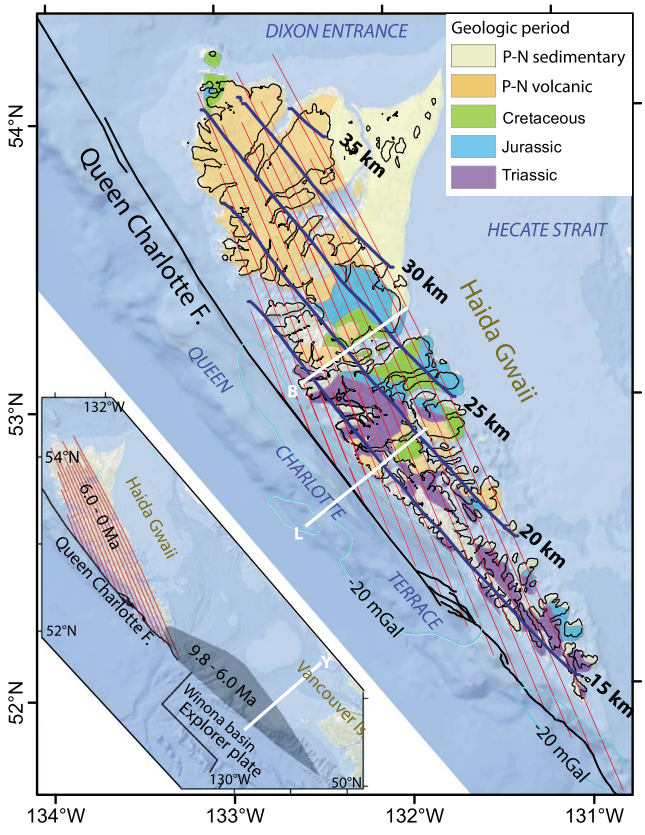

Figure 12. Predicted depth to the top of the slab under Haida Gwaii (heavy lines) and slab trajectory (parallel red lines), assuming a true underthrust dip of 5°, overlain on simplified geologic map of Haida Gwaii. Intrusive rocks are not shown on map. Map modified from Massey et al. (2005). P-N—Paleogene-Neogene. Black contour on Haida Gwaii—100-m elevation contour. White lines—locations of published estimates of top of underthrusted plate by (a) Lay et al. (2013) and (b) Bustin et al. (2007). Blue lines—contour enclosing negative residual free-air gravity anomaly of −20 mGal. Inset—predicted extent of underthrusted Pacific plate landward of Explorer plate following Hyndman's (2015) suggestion that the Queen Charlotte Fault extended south to northern Vancouver Island prior to 6 Ma. Ages are the time periods in which underthrusting at convergence angles >15° are predicted to have taken place. White line—location of Yuan et al. (1992) reflection, refraction, and gravity profile.

(Lay et al., 2013), the slab entry dip is 5°. Using the slab dip measured from receiver function analysis under the island (Bustin et al., 2007), 28.5°, gives an entry dip of 8° along the slab trajectory. These angles are similar to those found for slab angles under the Cascadia outer margin (≤4°, Flueh et al., 1998; 5°, McCrory et al., 2012).

Given the short duration of underthrusting and the low entry angle, the slab has probably not yet reached deep enough below the lithosphere (Figure 12) to generate mantle corner flow or generate arc volcanism. Hyndman (2015) proposed that Haida Gwaii is rising due to dynamic topography created during the first few million years of subduction initiation and cited a large positive gravity anomaly over Haida Gwaii as evidence. His suggestion followed the interpretation of a large positive Bouguer anomaly over Fiordland, New Zealand, as an indication for dynamic support during subduction initiation (House et al., 2002). However, the positive Bouguer gravity anomaly over Haida Gwaii is similar to the positive Bouguer anomaly observed farther north at the same distances from QCF (Figure 5b). (The positive anomaly landward of the fault is part of the gravity edge effect.) The slab top is expected to have only reached a maximum depth of 36 km (Figure 12), assuming a slab entry angle of 5° at a depth of 10 km. The slab could reach deeper if its dip increases after entry; however, receiver function interpretation Bustin et al. (2007) puts the top of the oceanic crust only 10 km deeper than predicted by a constant dip of 5°.

Uplift along Haida Gwaii's narrow ridge of high topography may take place as part of the underthrusting process, judging from the decreasing age of surface rocks from south to north along the spine of the archipelago (Figure 12; Hyndman & Hamilton, 1993). The area of Haida Gwaii overlying the slab could have undergone up to several kilometers of rock uplift with amplitudes decreasing from south to north along the island without a noticeable gravity anomaly. The lack of a distinct Bouguer gravity anomaly associated with the uplift (Figure 5b) is due to the fact that basement rocks landward of the QCF in both Haida Gwaii and southeastern Alaska have high density regardless of their age of emplacement. The older Wrangellia terrane rocks on Haida Gwaii are basalt flows and sedimentary rocks (e.g., Greene et al., 2010), whereas the northern third of Haida Gwaii is covered by the 35 to 20-Ma Massett basalt flows (e.g., Hyndman & Hamilton, 1993). High-density basement rocks also underlie the shelf off southeastern Alaska, which are Paleozoic Alexander terrane meta-volcanic and meta-sedimentary rocks with granodiorite intrusions (Gehrels & Saleeby, 1987). Given the expected high density of shallow rocks along the landward side of the QCF, the gravity field cannot be used to estimate the amount of basement uplift.

5.1.1. Unresolved Issues From the Underthrust Model

Despite the underthrusting, over 90% of the relative plate motion (~47 mm/yr) along Haida Gwaii is expected to be parallel to the fault (Figure 11d). However, the rake of the 2012 Haida Gwaii earthquake (103°, Lay et al., 2013) indicates that it had thrust motion, not oblique strike-slip motion, although most of the seismic slip took place seaward of QCF. If this is a typical earthquake for the region, it suggests the existence of slip partitioning between thrust and strike slip (Lay et al., 2013). If, as indicated by the rupture plane of the earthquake, the QCF does not cut through the top of Pacific oceanic crust, the strike-slip component of the motion must either be accommodated along the subhorizontal slab-top interface under the island (Lay et al., 2013) or along a yet-unknown strike-slip fault elsewhere. Thermal models suggest that the interface is within the ductile regime and is expected to slip aseismically and obliquely (Wang et al., 2015).

A convergence angle of 14° to 15° is too small to initiate underthrusting of the Pacific slab (e.g., McClay et al., 2004). Trehu et al. (2015) quoted analytical, numerical, and analog sand box models that show an initiation of

thrust faulting at obliquity angles of 15° to 25°. However, these models apply to strike-slip systems accompanied by subparallel thrust faults, not to underthrusting of a slab. Possible solutions to this mechanical problem include an upper crust with alternating elastic properties under Haida Gwaii and ductile lower crust, which can both provide reduced resistance to shear. Thick (~8-km total thickness) outcrops of horizontal to subhorizontal units of alternate composition (limestones, intrusives, mafic sills, and massive basalts) of Wranglia terrane are exposed in Alaska and British Columbia and underlie Haida Gwaii (Coney et al., 1980; Greene et al., 2010). Horizontal reflectors are observed within the crust underlying Hecate Strait (Spence & Asudeh, 1993), and receiver function analysis shows two crustal reflectivity peaks under Haida Gwaii (Bustin et al., 2007). Experimental rock mechanics data indicate a significant reduction in rock strength when the maximum compressive stress is inclined at 30 ± 15° to layering (Donath, 1961). Faults in a layered medium are composed of layer-parallel segments and layer-cutting ramps and may dip less than 25° from the maximum compressive stress (Peacock & Sanderson, 1992). Sibson (2012) documented many thrust earthquakes in the frontal Himalaya with low-dip (10 ± 5°) thrust mechanisms and proposed that they represent low-angle faults along bedding planes and ramps. Ductile deformation may also play a role. Considering the heat flow in the islands and their vicinity (~70 ± 10 mW/m^2, Smith et al., 2003) and the aforementioned lower crustal flow laws, we suggest that the crust below depths of 17.5–22 km under Haida Gwaii will deform ductily. Given the long history of plate subduction in the area, preserved ductile structures and layering parallel to the old descending Farallon slab may also be present in the overlying crust, which could promote underthrusting. Nevertheless, the reason for underthrusting at low oblique angles under the southern QCF remains poorly understood.

5.2. Contractional Deformation North of 53.1°N

The 2013 M_w 7.5 Craig earthquake and other earthquakes north of 53.1°N have strike-slip focal mechanisms, yet PA/NA relative motion is oblique to the QCF by 5° to 10° in this region (Figures 11a–11c and 11e). For example, the QCF at the latitude of the 2013 *M*7.5 Craig earthquake was under 4°–7° oblique convergence since the passage of the Yakutat terrane ~5 Ma (Figure 11e), resulting in a shortening component of 3–6 mm/yr (Figure 11b), and a total fault-perpendicular convergence of ~20–25 km. The convergence component north of 53.1°N could be accommodated by one or more of the following mechanisms: (1) buckling of the oceanic crust, (2) reactivation of abyssal hill fabric in the ocean crust as thrust faults, (3) a dipping strike-slip fault plane, (4) parallel thrust faults on the continental side of the fault, (5) an eastward displacement of the plate boundary, or (6) a northward translation or rotation of blocks inboard of the fault. Possible buckling of the oceanic crust (mechanism 1) is suggested by downward deflection of the crust in the gravity models (Figure 6a), although deflection could also arise from the loading of a broken elastic plate by sediments (Walton et al., 2015). Even if the bending is entirely due to buckling, downward deflection only accommodates ~0.1 km of perpendicular shortening along the profile crossing the 2013 Craig earthquake (Figure 6a). Reactivation of the oceanic crustal fabric adjacent to the fault by thrust faulting (mechanism 2) was identified in legacy seismic reflection profiles centered around 53.6° and 54.5°N (Trehu et al., 2015), but the amount of shortening was not estimated. One thrust aftershock of the 2013 Craig earthquake, was located ~23 km seaward of the fault (Holtkamp & Ruppert, 2015). Additional ridges, partially buried by slope sediments and oriented parallel to the seafloor fabric, were observed in seismic profiles between 55.4° and 57°N (Brothers et al., 2017; Bruns & Carlson, 1987; Walton et al., 2017). However, poor penetration, due to the high frequency of the sound source, does not permit deeper structural interpretation of these ridges.

Strike-slip motion during the 2013 Craig earthquake took place on a 75° to 80° eastward-dipping rupture plane (Figure 6a; mechanism 3). It is not known if the dip of the fault plane becomes progressively steeper farther south toward the underthrusting region of Haida Gwaii. A fault dip of 75° provides only 4 km of fault-perpendicular convergence at a crustal depth of 15 km. There are no documented active thrust faults on the continental side of the fault (mechanism 4) to suggest slip partitioning, except perhaps reactivation of early Miocene normal faults under Hecate Strait in a north-south compression (Rohr et al., 2000). Uplift along the fault trace itself is variable (Figure 13) and is smaller than the uplift predicted by the total convergence since the collapse of Southeastern Alaska ice cap (72 m at 5° convergence angle since 17,000 years), assuming that the seafloor morphology was reset by glacial erosion of the shelf and slope.

Comparison of the northward trajectory of the Yakutat terrane over the last 20 Ma to the present trace of the QCF shows a small discrepancy between 53.5° and 57.2°N, reaching a maximum of ~18 km at 55.0°N (Figure 9).

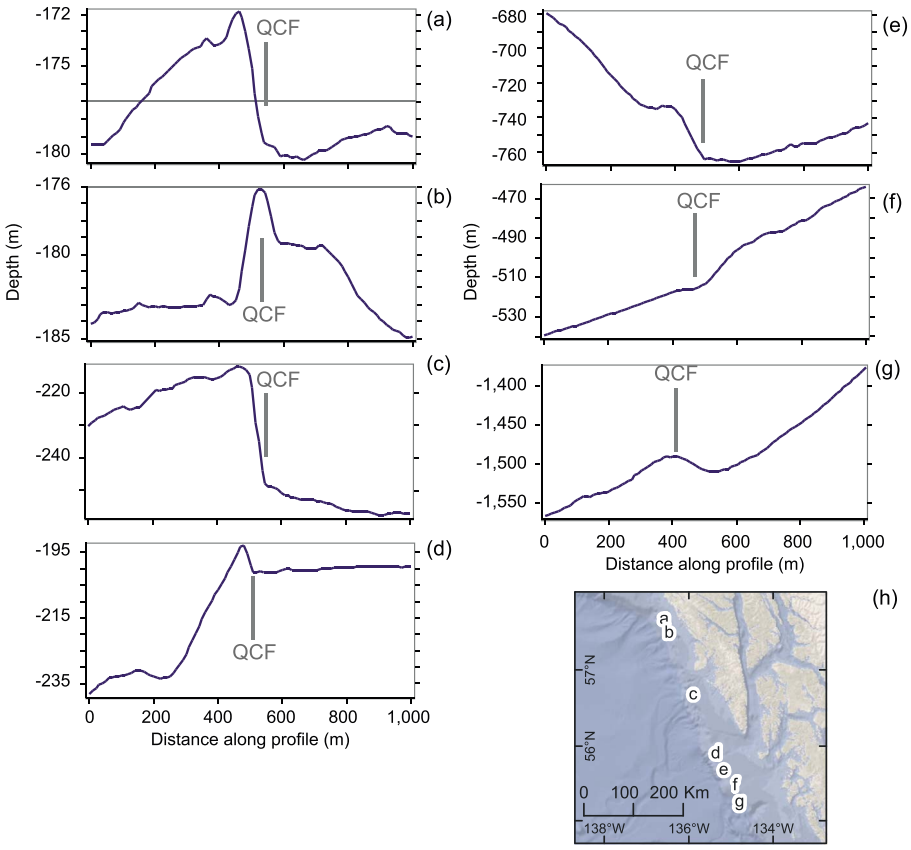

Figure 13. One thousand-meter-long bathymetric profiles across Queen Charlotte Fault at locations marked (a)–(g) in (h) and (e)–(g) in Figure 8a.

This discrepancy can either be attributed to uncertainty in the published stage poles of DeMets and Merkouriev (2016) or to an eastward displacement of the plate boundary itself (mechanism 5). An eastward displacement of the plate boundary can only occur if the North American side of the fault undergoes contraction, perhaps by block translation and rotation. Slip partitioning and block translation and rotation (mechanism 6) are common ways to accommodate oblique convergence (e.g., McCaffrey et al., 2007). Global Positioning System data indicate 2 to 3-mm/yr right-lateral motion on the Coast Shear Zone or on other inland faults (Elliott et al., 2010; Leonard et al., 2008; Mazzotti et al., 2008), which may help absorb the shortening component of deformation.

6. Conclusions

The QCF is in many respects an unusual transform plate boundary: Unlike similar plate boundaries, such as the PA/NA plate boundary in California, it is probably located along the COB. The expected contrast in elastic properties between oceanic and continental crust gives rise to unusual deformation styles. The PA/NA relative plate motion appears to be localized along a single, continuous linear fault, the QCF. The current slip rate along the fault is ~49 mm/yr, making the QCF the fastest moving nonoceanic strike-slip fault on Earth. We propose that the localization of relative plate motion along the modern singular QCF replaced earlier distributed motion in the former fore arc and arc regions as the Yakutat terrane migrated northward along the margin. The shortening component of deformation at convergence angles >14°–15° south of 53.1°N is accommodated by underthrusting of the Pacific plate under North America, leading perhaps to the uplift of Haida Gwaii. Overcoming frictional resistance and breaking a new low angle thrust interface may be facilitated by the combination of layered, mechanically anisotropic composition of the continental crust, inherited subduction features within the crust, and ductile lower crust. Shortening at smaller convergence angles is accommodated perhaps by a steeply dipping strike-slip fault plane, secondary small thrusts on the oceanic crust, and/or by minor right-lateral displacement far inland. Additional seismic, geodetic, and geological

observations are needed to verify some of the premises and constrain the unknowns discussed in this paper. Given the apparent simplicity of the deformation along this plate boundary and the high relative plate motion, we propose that QCF can be used as a natural laboratory to study the influence of crustal rheology on strike slip and transpressive deformation regimes and on the initiation of plate underthrusting.

Acknowledgments

Discussions with Jared Kluesner, Vaughn Barrie, Hohn Kao, Gary Greene, Janet Watt, Junbong Jang, and Bill Waite are gratefully acknowledged. We thank Tom Brocher, Debbie Hutchinson, the associate editor, and two anonymous reviewers for helpful reviews and the Captain and crew of the R/V *Medeia* for their support in the collection of multibeam bathymetry data. Relative plate motions are from DeMets and Merkouriev (2016, see reference list). Data sources for earthquake focal mechanisms, free-air gravity anomalies, multibeam bathymetry, and the geology of Haida Gwaii are listed in Figures 1, 2, 4, 8, and 12, respectively.

References

Atwater, T. (1989). Plate tectonic history of the Northeast Pacific and western North America. In E. L. Winterer, D. M. Hussong, & R. W. Decker (Eds.), *The eastern Pacific Ocean and Hawaii* (pp. 21–72). Boulder, CO: Geological Society of America, geology of North America.

Barrie, J. V., Conway, K. W., & Harris, P. T. (2013). The Queen Charlotte Fault, British Columbia: Seafloor anatomy of a transform fault and its influence on sediment processes. *Geo-Marine Letters*, *33*(4), 311–318. https://doi.org/10.1007/s00367-013-0333-3

Ben-Zion, Y. (2001). Dynamic ruptures in recent models of earthquake faults. *Journal of the Mechanics and Physics of Solids*, *49*(9), 2209–2244. https://doi.org/10.1016/S0022-5096(01)00036-9

Brace, W. F., & Kohlstedt, D. W. (1980). Limits on lithospheric stress imposed by laboratory measurements. *Journal of Geophysical Research*, *85*, 6248–6252. https://doi.org/10.1029/JB085iB11p06248

Brietzke, G. B., & Ben-Zion, Y. (2006). Examining tendencies of in-plane rupture to migrate to material interfaces. *Geophysical Journal International*, *167*(2), 807–819. https://doi.org/10.1111/j.1365-246X.2006.03137.x

Brothers, D., Haeussler, P., East, A., ten Brink, U. S., Andrews, B., Dartnell, P., et al. (2017). New seafloor imagery of the Queen Charlotte-Fairweather Fault System—"The San Andreas of the north". *Eos*, *98*. https://doi.org/10.1029/2017EO079019

Brothers, D. S., Elliott, J. L., Conrad, J. E., Haeussler, P. J., & Kluesner, J. W. (2018). Strain partitioning in southeastern Alaska: Is the Chatham Strait Fault active? *Earth and Planetary Science Letters*, *481*, 362–371. https://doi.org/10.1016/j.epsl.2017.10.017

Bruns, T., & Carlson, P. (1987). Geology and petroleum potential of the southeast Alaska continental margin. In D. W. Scholl, A. Grantz, & J. G. Vedder (Eds.), *Geology and resource potential of the continental margin of Western North America and adjacent ocean basins—Beaufort Sea to Baja California* (pp. 269–282). Houston: Circum-Pacific Council for Energy and Mineral Resources.

Bruns, T. R. (1983). Model for the origin of the Yakutat block, an accreting terrane in the northern Gulf of Alaska. *Geology*, *11*(12), 718–721. https%3A%2F%2Fdoi.org%2F10.1130%2F0091-7613(1983)11%253C718%3AMFTOOT%253E2.0.CO%3B2

Bruns, T. R., Stevenson, A. J., & Dobson, M. R. (1992). GLORIA investigation of the exclusive economic zone in the Gulf of Alaska and off southeast Alaska: M/V *Farnella* cruise F7-89-GA, June 14–July 13, 1989, U.S. Geol. Surv. Open-File Rept. 92-317, 16 pp.

Bustin, A. M. M., Hyndman, R. D., Kao, H., & Cassidy, J. F. (2007). Evidence for underthrusting beneath the Queen Charlotte Margin, British Columbia, from teleseismic receiver function analysis. *Geophysical Journal International*, *171*(3), 1198–1211. https://doi.org/10.1111/j.1365-246X.2007.03583.x

Chardon, D., Andronicos, C. L., & Hollister, L. S. (1999). Large-scale transpressive shear zone patterns and displacements within magmatic arcs: The Coast Plutonic Complex, British Columbia. *Tectonics*, *18*, 278–292. https://doi.org/10.1029/1998TC900035

Cobbett, R., Israel, S., Mortensen, J., Joyce, N., & Crowley, J. (2016). Structure and kinematic evolution of the Duke River fault, southwestern Yukon. *Canadian Journal of Earth Sciences*, *54*, 322–344.

Coney, P. J., Jones, D. L., & Monger, J. W. (1980). Cordilleran suspect terranes. *Nature*, *288*(5789), 329–333. https://doi.org/10.1038/288329a0

Davidson, C., Davis, K. J., Bailey, C. M., Tape, C. H., Singleton, J., & Singer, B. (2003). Age, origin, and significance of brittle faulting and pseudotachylyte along the coast shear zone, Prince Rupert, British Columbia. *Geology*, *31*(1), 43–46. https://doi.org/10.1130/0091-7613(2003)031%3C0043:AOASOB%3E2.0.CO;2

Davis, E., & Riddihough, R. (1982). The Winona Basin: Structure and tectonics. *Canadian Journal of Earth Sciences*, *19*(4), 767–788. https://doi.org/10.1139/e82-065

Dehler, S. A., & Clowes, R. M. (1988). The Queen Charlotte Islands refraction project. Part I. The Queen Charlotte Fault Zone. *Canadian Journal of Earth Sciences*, *25*(11), 1857–1870. https://doi.org/10.1139/e88-175

DeMets, C., & Merkouriev, S. (2016). High-resolution reconstructions of Pacific-North America plate motion: 20 Ma to present. *Geophysical Journal International*, *207*(2), 741–773. https://doi.org/10.1093/gji/ggw305

Dickinson, W. R., & Snyder, W. S. (1979). Geometry of subducted slabs related to San Andreas transform. *Journal of Geology*, *87*(6), 609–627. https://doi.org/10.1086/628456

Donath, F. A. (1961). Experimental study of shear failure in anisotropic rocks. *Geological Society of America Bulletin*, *72*(6), 985–989. https://doi.org/10.1130/0016-7606(1961)72%5B985:ESOSFI%5D2.0.CO;2

Doubrovine, P. V., & Tarduno, J. A. (2008). A revised kinematic model for the relative motion between Pacific oceanic plates and North America since the Late Cretaceous. *Journal of Geophysical Research*, *113*, B12101. https://doi.org/10.1029/2008JB005585

Eberhart-Phillips, D., Christensen, D. H., Brocher, T. M., Hansen, R., Ruppert, N. A., Haeussler, P. J., & Abers, G. A. (2006). Imaging the transition from Aleutian subduction to Yakutat collision in Central Alaska, with local earthquakes and active source data. *Journal of Geophysical Research*, *111*, B11303. https://doi.org/10.1029/2005JB004240

Edwards, B. R., & Russell, J. K. (2000). Distribution, nature, and origin of Neogene-Quaternary magmatism in the Northern Cordilleran Volcanic Province, Canada. *Geological Society of America Bulletin*, *112*(8), 1280–1295. https://doi.org/10.1130/0016-7606(2000)112%3C1280:DNAOON%3E2.0.CO;2

Elliott, J. L., Larsen, C. F., Freymueller, J. T., & Motyka, R. J. (2010). Tectonic block motion and glacial isostatic adjustment in Southeast Alaska and adjacent Canada constrained by GPS measurements. *Journal of Geophysical Research*, *115*, B09407. https://doi.org/10.1029/2009JB007139

Engebretson, D. C., Cox, A., & Gordon, R. G. (1985). Relative motions between oceanic and continental plates in the Pacific basin. *Geological Society Special Publication Journal*, *206*, 1–60.

Eyles, C. H., & Lagoe, M. B. (1998). Slump-generated megachannels in the Pliocene-Pleistocene glaciomarine Yakataga Formation, Gulf of Alaska. *Geological Society of America Bulletin*, *110*(3), 395–408. https://doi.org/10.1130/0016-7606(1998)110%3C0395:SGMITP%3E2.3.CO;2

Ferris, A., Abers, G. A., Christensen, D. H., & Veenstra, E. (2003). High resolution image of the subducted Pacific plate beneath Central Alaska, 50–150 km depth. *Earth and Planetary Science Letters*, *214*(3–4), 575–588. https://doi.org/10.1016/S0012-821X(03)00403-5

Flueh, E. R., Fisher, M. A., Bialas, J., Childs, J. R., Klaeschen, D., Kukowski, N., et al. (1998). New seismic images of the Cascadia subduction zone from cruise SO108—ORWELL. *Tectonophysics*, *293*(1-2), 69–84. https://doi.org/10.1016/S0040-1951(98)00091-2

Gehrels, G. E., & Saleeby, J. B. (1987). Geologic framework, tectonic evolution, and displacement history of the Alexander terrane. *Tectonics*, *6*, 151–173. https://doi.org/10.1029/TC006i002p00151

Greene, A. R., Scoates, J. S., Weis, D., Katvala, E. C., Israel, S., & Nixon, G. T. (2010). The architecture of oceanic plateaus revealed by the volcanic stratigraphy of the accreted Wrangellia oceanic plateau. *Geosphere*, *6*(1), 47–73. https://doi.org/10.1130/ges00212.1

Greene, H. G., Barrie, J. V., Brothers, D. S., Nishenko, S. P., Konway, K., & Enkin, R., et al. (2016). The Queen Charlotte-Fairweather Fault Zone—The knife-edged Pacific-North American plate boundary, AGU Fall Meeting Abstract OS12B-08.

Haeussler, P. J., Bradley, D. C., Wells, R. E., & Miller, M. L. (2003). Life and death of the resurrection plate: Evidence for its existence and subduction in the northeastern Pacific in Paleocene-Eocene time. *Geological Society of America Bulletin*, *115*(7), 867–880. https://doi.org/10.1130/0016-7606(2003)115%3C0867:LADOTR%3E2.0.CO;2

Hetherington, R., & Barrie, J. V. (2004). Interaction between local tectonics and glacial unloading on the Pacific margin of Canada. *Quaternary International*, *120*(1), 65–77. https://doi.org/10.1016/j.quaint.2004.01.007

Hirth, G., & Kohlstedt, D. (2003). Rheology of the upper mantle and the mantle wedge: A view from the experimentalists. *Inside the subduction Factory*, 83–105. https://doi.org/10.1029/138GM06

Hollister, L. S., Diebold, J., & Das, T. (2008). Whole crustal response to late Tertiary extension near Prince Rupert, British Columbia. *Geosphere*, *4*(2), 360. https://doi.org/10.1130/ges000144.1

Holtkamp, S., & Ruppert, N. (2015). A high resolution aftershock catalog of the magnitude 7.5 Craig, Alaska, earthquake on 5 January 2013. *Bulletin of the Seismological Society of America*, *105*(2B), 1143–1152. https://doi.org/10.1785/0120140179

Horn, J. R., Clowes, R. M., Ellis, R. M., & Bird, D. N. (1984). The seismic structure across an active oceanic/continental transform fault zone. *Journal of Geophysical Research*, *89*, 3107–3120. https://doi.org/10.1029/JB089iB05p03107

House, M. A., Gurnis, M., Kamp, P. J., & Sutherland, R. (2002). Uplift in the Fiordland region, New Zealand: Implications for incipient subduction. *Science*, *297*(5589), 2038–2041. https://doi.org/10.1126/science.1075328

Hudson, T., Plafker, G., & Dixon, K. (1982). Horizontal offset history of the Chatham Strait fault, the U.S. survey in Alaska: Accomplishments during 1980. W. L. Coonrad. U.S. Geological Survey Circular 844: 12S132.

Hyndman, R. D. (2015). Tectonics and structure of the Queen Charlotte Fault Zone, Haida Gwaii, and large thrust earthquakes. *Bulletin of the Seismological Society of America*, *105*(2B), 1058–1075. https://doi.org/10.1785/0120140181

Hyndman, R. D., & Hamilton, T. S. (1993). Queen Charlotte area Cenozoic tectonics and volcanism and their association with relative plate motions along the northeastern Pacific margin. *Journal of Geophysical Research*, *98*, 14,257–14,277. https://doi.org/10.1029/93JB00777

Kao, H., Shan, S. J., & Farahbod, A. M. (2015). Source characteristics of the 2012 Haida Gwaii earthquake sequence. *Bulletin of the Seismological Society of America*, *105*(2B), 1206–1218. https://doi.org/10.1785/0120140165

Kaufman, D. S., & Manley, W. F. (2004). Pleistocene maximum and late Wisconsin glacier extents across Alaska, U.S.A. In J. Ehlers & P. L. Gibbard (Eds.), *Quaternary glaciations—Extent and chronology, part II: North America. Developments in quaternary science* (Chap. 2, pp. 9–27). Amsterdam: Elsevier. https://doi.org/10.1016/S1571-0866(04)80182-9

Lachenbruch, A. H. (1970). Crustal temperature and heat production: Implications of the linear heat-flow relation. *Journal of Geophysical Research*, *75*, 3291–3300. https://doi.org/10.1029/JB075i017p03291

Lay, T., Ye, L., Kanamori, H., Yamazaki, Y., Cheung, K. F., Kwong, K., & Koper, K. D. (2013). The October 28, 2012 Mw 7.8 Haida Gwaii underthrusting earthquake and tsunami: Slip partitioning along the Queen Charlotte Fault transpressional plate boundary. *Earth and Planetary Science Letters*, *375*, 57–70. https://doi.org/10.1016/j.epsl.2013.05.005

Leonard, L. J., Mazzotti, S., & Hyndman, R. D. (2008). Deformation rates estimated from earthquakes in the Northern Cordillera of Canada and eastern Alaska. *Journal of Geophysical Research*, *113*, B08406. https://doi.org/10.1029/2007JB005456

Lewis, T., Hyndman, R., & Flück, P. (2003). Heat flow, heat generation, and crustal temperatures in the northern Canadian Cordillera: Thermal control of tectonics. *Journal of Geophysical Research*, *108*(B6), 2316. https://doi.org/10.1029/2002JB002090

Lyles, A. S., Baichtal, J. F., & Karl, S. M. (2017). Deciphering flow path of ice across the southern Alaska panhandle based on geomorphological interpretation and field data. *Geological Society of America Abstracts with Programs*, *49*(6). https://doi.org/10.1130/abs/2017AM-304449

Mackwell, S. J., Zimmerman, M. E., & Kohlstedt, D. L. (1998). High-temperature deformation of dry diabase with application to tectonics on Venus. *Journal of Geophysical Research*, *103*, 975–984. https://doi.org/10.1029/97JB02671

Madsen, J. K., Thorkelson, D. J., Friedman, R. M., & Marshall, D. D. (2006). Cenozoic to recent plate configurations in the Pacific Basin: Ridge subduction and slab window magmatism in western North America. *Geosphere*, *2*(1), 11. https://doi.org/10.1130/ges00020.1

Massey, N. W. D., MacIntyre, D. G., Haggart, J. W., Desjardins, P. J., Wagner, C. L., & Cooney, R. T. (2005). Digital map of British Columbia: Tile NN8–9 North Coast and Queen Charlotte Islands/Haida Gwaii, B.C. Ministry of Energy and Mines, GeoFile 2005–2005.

Mazzotti, S., Leonard, L. J., Hyndman, R. D., & Cassidy, J. F. (2008). Tectonics, dynamics, and seismic hazard in the Canada-Alaska Cordillera. In J. T. Freymueller, P. J. Haeussler, R. L. Wesson, & G. Ekström (Eds.), *Active tectonics and seismic potential of Alaska* (pp. 297–319). Washington, DC: American Geophysical Union. https://doi.org/10.1029/179GM17

McCaffrey, R., Qamar, A. I., King, R. W., Wells, R., Khazaradze, G., Williams, C. A., et al. (2007). Fault locking, block rotation and crustal deformation in the Pacific Northwest. *Geophysical Journal International*, *169*(3), 1315–1340. https://doi.org/10.1111/j.1365-246X.2007.03371.x

McClay, K., Whitehouse, P., Dooley, T., & Richards, M. (2004). 3D evolution of fold and thrust belts formed by oblique convergence. *Marine and Petroleum Geology*, *21*(7), 857–877. https://doi.org/10.1016/j.marpetgeo.2004.03.009

McCrory, P. A., Blair, J. L., Waldhauser, F., & Oppenheimer, D. H. (2012). Juan de Fuca slab geometry and its relation to Wadati-Benioff zone seismicity. *Journal of Geophysical Research*, *117*, B09306. https://doi.org/10.1029/2012JB009407

McKenzie, D., & Bickle, M. (1988). The volume and composition of melt generated by extension of the lithosphere. *Journal of Petrology*, *29*(3), 625–679. https://doi.org/10.1093/petrology/29.3.625

Miller, N. C., & Behn, M. D. (2012). Timescales for the growth of sediment diapirs in subduction zones. *Geophysical Journal International*, *190*(3), 1361–1377. https://doi.org/10.1111/j.1365-246X.2012.05565.x

Molnia, B. F. (1986). Glacial history of the northeastern Gulf of Alaska—A synthesis. In T. D. Hamilton, K. M. Reed, & R. M. Thorson (Eds.), *Glaciation in Alaska: The geologic record* (pp. 219–235). Anchorage: Alaska Geological Society.

Morozov, I. B., Smithson, S. B., Chen, J., & Hollister, L. S. (2001). Generation of new continental crust and terrane accretion in southeastern Alaska and western British Columbia: Constraints from P- and S-wave wide-angle seismic data (ACCRETE). *Tectonophysics*, *341*(1–4), 49–67.

Peacock, D., & Sanderson, D. (1992). Effects of layering and anisotropy on fault geometry. *Journal of the Geological Society*, *149*(5), 793–802. https://doi.org/10.1144/gsjgs.149.5.0793

Powell, R. D., & Molnia, B. F. (1989). Glacimarine sedimentary processes, facies and morphology of the south-southeast Alaska shelf and fjords. *Marine Geology*, *85*(2-4), 359–390. https://doi.org/10.1016/0025-3227(89)90160-6

Ranalli, G. (1995). *Rheology of the Earth*. London: Chapman and Hall.

Richter, D., & Matson, N. (1971). Quaternary faulting in the Eastern Alaska Range. *Geological Society of America Bulletin*, *82*(6), 1529–1540. https://doi.org/10.1130/0016-7606(1971)82%5B1529:QFITEA%5D2.0.CO;2

Ristau, J., Rogers, G. C., & Cassidy, J. F. (2007). Stress in western Canada from regional moment tensor analysis. *Canadian Journal of Earth Sciences*, *44*(2), 127–148. https://doi.org/10.1139/e06-057

Rohr, K., & Dietrich, J. (1992). Strike-slip tectonics and development of the Tertiary Queen Charlotte Basin, offshore western Canada: Evidence from seismic reflection data. *Basin Research*, *4*(1), 1–20. https://doi.org/10.1111/j.1365-2117.1992.tb00039.x

Rohr, K. M., & Furlong, K. P. (1995). Ephemeral plate tectonics at the Queen Charlotte triple junction. *Geology*, *23*(11), 1035–1038. https://doi.org/10.1130/0091-7613(1995)023%3C1035:EPTATQ%3E2.3.CO;2

Rohr, K. M. M., Scheidhauer, M., & Trehu, A. M. (2000). Transpression between two warm mafic plates: The Queen Charlotte Fault revisited. *Journal of Geophysical Research*, *105*, 8147–8172. https://doi.org/10.1029/1999JB900403

Rybacki, E., & Dresen, G. (2000). Dislocation and diffusion creep of synthetic anorthite aggregates. *Journal of Geophysical Research*, *105*, 26,017–26,036. https://doi.org/10.1029/2000JB900223

Seton, M., Müller, R., Zahirovic, S., Gaina, C., Torsvik, T., Shephard, G., et al. (2012). Global continental and ocean basin reconstructions since 200 Ma. *Earth Science Reviews*, *113*(3–4), 212–270. https://doi.org/10.1016/j.earscirev.2012.03.002

Sibson, R. (2012). Reverse fault rupturing: Competition between non-optimal and optimal fault orientations. *Geological Society, London, Special Publications*, *367*(1), 39–50. https://doi.org/10.1144/SP367.4

Smith, A. J., Hyndman, R. D., Cassidy, J. F., & Wang, K. (2003). Structure, seismicity, and thermal regime of the Queen Charlotte transform margin. *Journal of Geophysical Research*, *108*(B11), 2539. https://doi.org/10.1029/2002JB002247

Spence, G., & Asudeh, I. (1993). Seismic velocity structure of the Queen Charlotte basin beneath Hecate Strait. *Canadian Journal of Earth Sciences*, *30*(4), 787–805. https://doi.org/10.1139/e93-065

Steckler, M. S., & ten Brink, U. S. (1986). Lithospheric strength variations as a control on new plate boundaries: Examples from the northern Red Sea region. *Earth and Planetary Science Letters*, *79*(1-2), 120–132. https://doi.org/10.1016/0012-821X(86)90045-2

Stock, J., & Molnar, P. (1988). Uncertainties and implications of the Late Cretaceous and Tertiary position of North America relative to the Farallon, Kula, and Pacific plates. *Tectonics*, *7*, 1339–1384. https://doi.org/10.1029/TC007i006p01339

Trehu, A. M., Scheidhauer, M., Rohr, K. M. M., Tikoff, B., Walton, M. A. L., Gulick, S. P. S., & Roland, E. C. (2015). An abrupt transition in the mechanical response of the upper crust to transpression along the Queen Charlotte Fault. *Bulletin of the Seismological Society of America*, *105*(2B), 1114–1128. https://doi.org/10.1785/0120140159

Trop, J. M., Hart, W. K., Snyder, D., & Idleman, B. (2012). Miocene basin development and volcanism along a strike-slip to flat-slab subduction transition: Stratigraphy, geochemistry, and geochronology of the Central Wrangell volcanic belt, Yakutat-North America collision zone, geosphere, GES00762. 00,761.

Vink, G. E., Morgan, W. J., & Zhao, W.-L. (1984). Preferential rifting of continents—A source of displaced terranes. *Journal of Geophysical Research*, *89*, 10,072–10,076. https://doi.org/10.1029/JB089iB12p10072

Walton, M., Miller, N., Brothers, D., Kluesner, J., Haeussler, P., Conrad, J., et al. (2017). New evidence for quaternary strain partitioning along the Queen Charlotte Fault system, southeeastern Alaska, AGU Fall Meeting Abstract T51G-0558.

Walton, M. A. L., Gulick, S. P. S., Haeussler, P. J., Roland, E. C., & Trehu, A. M. (2015). Basement and regional structure along strike of the Queen Charlotte Fault in the context of modern and historical earthquake ruptures. *Bulletin of the Seismological Society of America*, *105*(2B), 1090–1105. https://doi.org/10.1785/0120140174

Wang, K., He, J., Schulzeck, F., Hyndman, R. D., & Riedel, M. (2015). Thermal condition of the 27 October 2012 Mw 7.8 Haida Gwaii subduction earthquake at the obliquely convergent Queen Charlotte margin. *Bulletin of the Seismological Society of America*, *105*(2B), 1290–1300. https://doi.org/10.1785/0120140183

Weertman, J. (1980). Unstable slippage across a fault that separates elastic media of different elastic constants. *Journal of Geophysical Research*, *85*, 1455–1461. https://doi.org/10.1029/JB085iB03p01455

Wells, R., Bukry, D., Friedman, R., Pyle, D., Duncan, R., Haeussler, P., & Wooden, J. (2014). Geologic history of Siletzia, a large igneous province in the Oregon and Washington Coast Range: Correlation to the geomagnetic polarity time scale and implications for a long-lived Yellowstone hotspot. *Geosphere*, *10*(4), 692–719. https://doi.org/10.1130/ges01018.1

White, T., Bradley, D., Haeussler, P., & Rowley, D. B. (2017). Late Paleocene-early Eocene Paleosols and a new measure of the transport distance of Alaska's Yakutat terrane. *The Journal of Geology*, *125*(2), 113–123. https://doi.org/10.1086/690198

Worthington, L. L., Van Avendonk, H. J. A., Gulick, S. P. S., Christeson, G. L., & Pavlis, T. L. (2012). Crustal structure of the Yakutat terrane and the evolution of subduction and collision in southern Alaska. *Journal of Geophysical Research*, *117*, B01102. https://doi.org/10.1029/2011JB008493

Wyld, S. J., Umhoefer, P. J., & Wright, J. E. (2006). Reconstructing northern cordilleran terranes along known Cretaceous and Cenozoic strike-slip faults: Implications for the Baja British Columbia hypothesis and other models, in: J. W. Haggart, et al. (eds.) Paleogeography of the North American cordillera: Evidence for and against large-scale displacements. *Geological Association of Canada Special Paper*, *46*, 277–298.

Yuan, T., Spence, G., & Hyndman, R. (1992). Structure beneath Queen Charlotte Sound from seismic-refraction and gravity interpretations. *Canadian Journal of Earth Sciences*, *29*(7), 1509–1529. https://doi.org/10.1139/e92-120

Yue, H., Lay, T., Freymueller, J. T., Ding, K., Rivera, L., Ruppert, N. A., & Koper, K. D. (2013). Supershear rupture of the 5 January 2013 Craig, Alaska (Mw 7.5) earthquake. *Journal of Geophysical Research: Solid Earth*, *118*, 5903–5919. https://doi.org/10.1002/2013JB010594